Journal of Modern Optics

ISSN: 0950-0340 (Print) 1362-3044 (Online) Journal homepage: www.tandfonline.com/journals/tmop20

Squeezed Light

R. Loudon & P.L. Knight

To cite this article: R. Loudon & P.L. Knight (1987) Squeezed Light, Journal of Modern Optics, 34:6-7, 709-759, DOI: 10.1080/09500348714550721

To link to this article: https://doi.org/10.1080/09500348714550721

Published online: 01 Mar 2007.

JOURNAL OF MODERN OPTICS, 1987, VOL. 34, NOS. 6/7, 709–759

Squeezed light

R. LOUDON
Physics Department, Essex University,
Colchester CO4 3SQ, England

and P. L. KNIGHT
Optics Section, Blackett Laboratory,
Imperial College, London SW7 2BZ, England

Abstract. In this paper we review the current state of progress in research on squeezed light. We discuss the basic theory of squeezing and the nature of quantum noise in optical fields. We examine various atomic sources of squeezed light and discuss phase-sensitive detectors of quantum noise including homodyne and heterodyne detectors. Various successful nonlinear optical methods for generating squeezed light are reviewed. We conclude with a discussion of the possible applications of squeezed light.

1. Introduction

All light fields fluctuate: their amplitudes and phases are subject to a stochastic indeterminacy. Much of this indeterminacy in practical light sources derives from environmental influences. For example, radiating atoms can collide with other atoms so that the phase of the emitted light is disrupted, optical components in a light source can vibrate in an uncontrolled fashion and lead to random changes in frequency and amplitude, and the rate of atomic excitation in any light source can vary in a random way. These factors can in principle be eliminated by a careful design of the light source. Even if all of these influences are removed, however, we are left with a more fundamental kind of optical noise. Optical fields obey the laws of quantum mechanics and have an inherent quantum indeterminacy which cannot be removed no matter how carefully the light source is controlled. A measure of the minimum size of this quantum optical noise for a single-mode field of frequency ω is given by the quantity

$$\mathscr{E}_0 = (\hbar\omega/2\varepsilon_0 V)^{1/2}, \tag{1.1}$$

where V is the volume over which the field is excited. This noise has the same magnitude for any strength of excitation of the field mode: indeed the same size of field fluctuation is present even in the absence of any field excitation. For this reason, $\mathscr{E}_0$ is often associated with the vacuum fluctuations of the electromagnetic field.

A classical coherent electromagnetic field varies sinusoidally with phase angle, with a precisely defined amplitude. A quantized coherent field, on the other hand, has an uncertainty $\mathscr{E}_0$ in the magnitude of its amplitude, irrespective of phase angle. In figure 1 we show the variation of the mean amplitude of a quantized coherent field with phase angle, indicated by the dashed line, with the size of the fluctuations

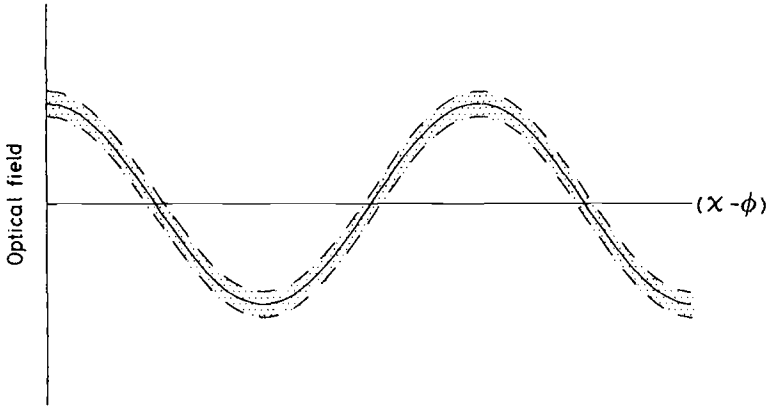

Figure 1. Phase dependence of the mean field and its uncertainty for coherent light. The vertical width of the shaded region indicates the square root of the variance of the optical field amplitude.

around the mean indicated by the shaded band. In contrast, recent work on 'squeezed states' of the light field (reviewed for example in [1–4]) has uncovered ways in which the electric field uncertainty may be reduced *below* $\mathscr{E}_0$ for certain values of the phase angle, with a concomitant increase in field uncertainty at complementary phase angles. In figure 2 we show the variation with phase angle of the noise properties of one type of squeezed state, with the same mean amplitude as that of the coherent state in figure 1. The phase angles for minimum uncertainty in this example have been chosen to demonstrate the squeezing of the amplitude fluctuations; note that the accuracy to which the phase can be determined has been reduced compared to the coherent state. For example, amplitude squeezing may be produced by an interaction which depends quadratically on field amplitude, and which preferentially removes the large amplitude fluctuations, to result in a radiation field quieter than the vacuum. This possibility for obtaining light whose amplitude fluctuations are less than those expected from shot noise considerations has attracted a great deal of attention. Squeezing is an important addition to the class of effects requiring field quantization for their explanation [5]. This special issue and this review article are concerned with the properties of squeezed light.

Squeezed states of light were first studied by theorists interested in their properties as generalized minimum-uncertainty states [6–14]. These properties were discovered independently by several workers using different terminologies and have been described variously as 'pulsating wave packets' [6], 'new coherent states' [10, 11], 'two-photon coherent states' [12] and 'ideal squeezed states' [14]. The first experimental realization of squeezed light was reported by Slusher and coworkers [15] using four-wave mixing in sodium atoms. They were able to reduce the optical noise below the vacuum fluctuation level by 7 to 10 per cent using a combination of phase-stable laser excitation and cavity field enhancement. Four-wave mixing in an optical fibre was used by Shelby and coworkers [16] to generate squeezed light, with a $12\frac{1}{2}$ per cent reduction below the vacuum noise value. Wu and coworkers have reported the largest value of squeezing observed so far [17]. They use a parametric

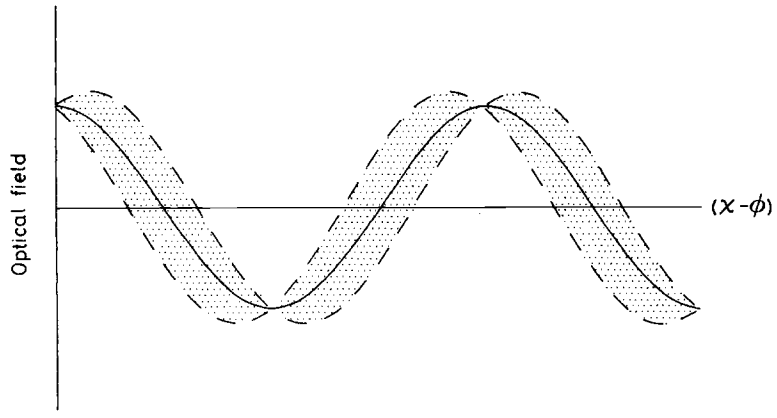

Figure 2. Phase dependence of the mean field and its uncertainty for squeezed light. The mean photon number $|\alpha|^2=4$ as in figure 1, the phase $\phi=\frac{1}{2}\theta$ and the squeeze parameter, defined in § 2.5, is chosen to be $s=1{\cdot}5$.

down-conversion process to produce highly correlated pairs of photons at the subharmonic frequency of the pump laser and observe 63 per cent noise reduction. Clearly vacuum fluctuations can now be manipulated at will by the nonlinear-optical scientist.

2. Variances, fluctuations and squeezing

2.1. *Quantum fluctuations of light*

A single cavity mode of the electromagnetic field behaves like a simple harmonic oscillator of unit mass and is described by the 'position' and 'momentum' operators $\hat{q}$ and $\hat{p}$ related to the conjugate electric and magnetic field operators $\hat{E}$ and $\hat{H}$. If we assume the radiation field is confined in a one-dimensional cavity whose axis is parallel to the z-axis, and is linearly polarized, we can write [18]

$$\hat{E}(z,t)=(2\omega^2/\varepsilon_0 V)^{1/2}\hat{q}(t)\sin kz, \tag{2.1}$$

$$\hat{H}(z,t)=(2\varepsilon_0 c^2/V)^{1/2}\hat{p}(t)\cos kz, \tag{2.2}$$

where the wave-vector $k=\omega/c$, and V is the quantization volume of the cavity. The operators $\hat{p}$ and $\hat{q}$ obey the equal-time commutation relation $[\hat{p}(t),\hat{q}(t)]=-\mathrm{i}\hbar$. It is convenient to introduce the non-Hermitian combinations of $\hat{p},\hat{q}$:

$$\hat{a}=(2\hbar\omega)^{-1/2}(\omega\hat{q}+\mathrm{i}\hat{p}), \tag{2.3}$$

$$\hat{a}^\dagger=(2\hbar\omega)^{-1/2}(\omega\hat{q}-\mathrm{i}\hat{p}), \tag{2.4}$$

where $\hat{a}$ is the destruction operator and $\hat{a}^\dagger$ the creation operator. The corresponding commutation relation is $[\hat{a},\hat{a}^\dagger]=1$. The electric-field operator for the cavity mode of frequency ω can be written as

$$\hat{E}(z,t)=\tfrac{1}{2}\mathscr{E}_c\{\hat{a}(t)+\hat{a}^\dagger(t)\}, \tag{2.5}$$

where $\mathscr{E}_c$ is the natural unit of electric field strength in the cavity,

$$\mathscr{E}_c=2^{3/2}\mathscr{E}_0\sin kz, \tag{2.6}$$

$\mathscr{E}_0$ is the 'electric field per photon' given by equation (1.1) and $\hat{a}(t)=\hat{a}(0)\exp(-\mathrm{i}\omega t)$.

The destruction and creation operators act on photon number states in the normal way [19],

$$\hat{a}|n\rangle = n^{1/2}|n-1\rangle, \tag{2.7a}$$

$$\hat{a}^\dagger|n\rangle = (n+1)^{1/2}|n+1\rangle, \tag{2.7b}$$

so that the number state can be written in terms of the vacuum state as

$$|n\rangle = (n!)^{-1/2}(\hat{a}^\dagger)^n|0\rangle. \tag{2.8}$$

Fluctuations in observables $\hat{O}$ are described by the variance, defined by

$$\langle(\Delta O)^2\rangle \equiv \langle\hat{O}^2\rangle - \langle\hat{O}\rangle^2, \tag{2.9}$$

where for brevity we have written $\langle\hat{O}\rangle$ for $\langle\psi|\hat{O}|\psi\rangle$, and note that the variance is a state-dependent quantity. We note that the variances $\langle(\Delta A)^2\rangle$ and $\langle(\Delta B)^2\rangle$ of two observable quantities for the same state $|\psi\rangle$ satisfy the uncertainty relation

$$\langle(\Delta A)^2\rangle\langle(\Delta B)^2\rangle \geqslant \tfrac{1}{4}|\langle[\hat{A},\hat{B}]\rangle|^2, \tag{2.10}$$

and if the equality sign holds, the states $|\psi\rangle$ are denoted 'minimum uncertainty states' (MUS). It is simple to show that the ground state of the single-mode radiation field, $|0\rangle$, is a minimum-uncertainty state for the operators $\hat{p}$ and $\hat{q}$ (or equivalently $\hat{a}$ and $\hat{a}^\dagger$). We have

$$\langle 0|\hat{p}|0\rangle = \langle 0|\hat{q}|0\rangle = 0 \tag{2.11}$$

and

$$\langle(\Delta q)_0^2\rangle = \langle 0|\hat{q}^2|0\rangle = \left\langle 0\left|\left(\frac{\hbar}{2\omega}\right)(\hat{a}+\hat{a}^\dagger)(\hat{a}+\hat{a}^\dagger)\right|0\right\rangle = \hbar/2\omega. \tag{2.12}$$

Similarly

$$\langle(\Delta p)_0^2\rangle = \langle 0|\hat{p}^2|0\rangle = \hbar\omega/2. \tag{2.13}$$

Thus

$$\langle(\Delta p)_0^2\rangle\langle(\Delta q)_0^2\rangle = (\hbar/2)^2, \tag{2.14}$$

in agreement with equation (2.10) with the equality sign, since the relevant commutator in this case is simply $-i\hbar$.

The coherent states $|\alpha\rangle$ are right eigenstates of the destruction operator $\hat{a}$:

$$\hat{a}|\alpha\rangle = \alpha|\alpha\rangle, \tag{2.15}$$

where α is a complex amplitude $\alpha = |\alpha|\exp(i\phi)$. In terms of the number states $|n\rangle$,

$$|\alpha\rangle = \exp(-\tfrac{1}{2}|\alpha|^2)\sum_{n=0}^{\infty}\frac{\alpha^n}{(n!)^{1/2}}|n\rangle. \tag{2.16}$$

The photon number variance for a single-mode coherent state is, using $\hat{n} \equiv \hat{a}^\dagger\hat{a}$ and equation (2.15), given by

$$\langle(\Delta n)^2\rangle = \langle\hat{n}^2\rangle - \langle\hat{n}\rangle^2 = |\alpha|^2 = \langle\hat{n}\rangle, \tag{2.17}$$

where $|\alpha|^2$ is the mean number of photons in the coherent state. The expectation

values of the position and momentum operators are non-zero for a coherent state,

$$\langle\alpha|\hat{q}|\alpha\rangle=(\hbar/2\omega)^{1/2}(\alpha+\alpha^*), \tag{2.18a}$$

$$\langle\alpha|\hat{p}|\alpha\rangle=\mathrm{i}(\hbar\omega/2)^{1/2}(\alpha-\alpha^*), \tag{2.18b}$$

and for the squares of the operators,

$$\langle\alpha|\hat{q}^2|\alpha\rangle=(\hbar/2\omega)[\alpha^2+(\alpha^*)^2+2|\alpha|^2+1], \tag{2.19a}$$

$$\langle\alpha|\hat{p}^2|\alpha\rangle=-(\hbar\omega/2)[\alpha^2+(\alpha^*)^2-2|\alpha|^2-1]. \tag{2.19b}$$

We find, therefore, from the coherent-state variances

$$\langle(\Delta q)_\alpha^2\rangle=\hbar/2\omega \tag{2.20}$$

and

$$\langle(\Delta p)_\alpha^2\rangle=\hbar\omega/2, \tag{2.21}$$

that the coherent states, irrespective of their degree of excitation, are MUS:

$$\langle(\Delta q)_\alpha^2\rangle\langle(\Delta p)_\alpha^2\rangle=(\hbar/2)^2. \tag{2.22}$$

The minimum-uncertainty state is a Gaussian wavepacket in position space,

$$\psi(q)=\langle q|\alpha\rangle=C\exp(-q^2/4\langle(\Delta q)_\alpha^2\rangle) \tag{2.23}$$

and also in momentum space

$$\begin{aligned}\psi(p)=\langle p|\alpha\rangle&=C'\exp(-p^2/4\langle(\Delta p)_\alpha^2\rangle)\\&=C'\exp(-p^2\langle(\Delta q)_\alpha^2\rangle/\hbar^2),\end{aligned} \tag{2.24}$$

where C and C' are normalization constants. A broad MUS wavepacket in position space corresponds to a narrow distribution in momentum space.

2.2. *Quadrature operators*

Because $\hat{q}$ and $\hat{p}$ have different dimensions, it is convenient to replace them by the quadrature operators

$$\hat{X}=\tfrac{1}{2}(\hat{a}+\hat{a}^\dagger)=(\omega/2\hbar)^{1/2}\hat{q} \tag{2.25}$$

and

$$\hat{Y}=\frac{1}{2\mathrm{i}}(\hat{a}-\hat{a}^\dagger)=(2\hbar\omega)^{-1/2}\hat{p}. \tag{2.26}$$

The cavity electric-field operator in terms of the quadrature operators is

$$\begin{aligned}\hat{E}(z,t)&=\tfrac{1}{2}\mathscr{E}_c[\hat{a}\exp(-\mathrm{i}\omega t)+\hat{a}^\dagger\exp(\mathrm{i}\omega t)]\\&=\mathscr{E}_c(\hat{X}\cos\omega t+\hat{Y}\sin\omega t).\end{aligned} \tag{2.27}$$

The quadrature operators satisfy the commutation relation

$$[\hat{X},\hat{Y}]=\mathrm{i}/2 \tag{2.28}$$

and their variances satisfy the uncertainty relation

$$\langle(\Delta X)^2\rangle\langle(\Delta Y)^2\rangle\geqslant 1/16. \tag{2.29}$$

For a coherent state (or for the special case of the vacuum state), the variances of the quadrature operators are equal:

$$\langle(\Delta X)_\alpha^2\rangle = \langle(\Delta Y)_\alpha^2\rangle = 1/4. \tag{2.30}$$

In figure 3 we represent the mean amplitude and the associated uncertainties for a coherent state by an error circle centred on the complex amplitude vector α. The diameter of the shaded area corresponds to the size of the quadrature-operator uncertainty. The centre of the uncertainty 'circle' is given by

$$\langle(\hat{X} + i\hat{Y})_\alpha\rangle = \alpha. \tag{2.31}$$

The coherent states can be generated from the vacuum states by the action of the Glauber unitary displacement operator [20, 21] according to

$$|\alpha\rangle = \hat{D}(\alpha)|0\rangle, \tag{2.32}$$

where

$$\hat{D}(\alpha) = \exp(\alpha\hat{a}^\dagger - \alpha^*\hat{a}). \tag{2.33}$$

The displacement operator produces the transformations

$$\left.\begin{aligned} \hat{a} &\to \hat{D}^{-1}(\alpha)\hat{a}\hat{D}(\alpha) = \hat{a} + \alpha, \\ \hat{a}^\dagger &\to \hat{D}^{-1}(\alpha)\hat{a}^\dagger\hat{D}(\alpha) = \hat{a}^\dagger + \alpha^*. \end{aligned}\right\} \tag{2.34}$$

In terms of the quadrature operators, the displacement operator

$$\hat{D}(\alpha) = \exp[2i(\operatorname{Im}\alpha\hat{X} - \operatorname{Re}\alpha\hat{Y})] \tag{2.35}$$

acts as a translation operator so that

$$\left.\begin{aligned} \hat{X} &\to \hat{D}^{-1}(\alpha)\hat{X}\hat{D}(\alpha) = \hat{X} + \operatorname{Re}\alpha, \\ \hat{Y} &\to \hat{D}^{-1}(\alpha)\hat{Y}\hat{D}(\alpha) = \hat{Y} + \operatorname{Im}\alpha. \end{aligned}\right\} \tag{2.36}$$

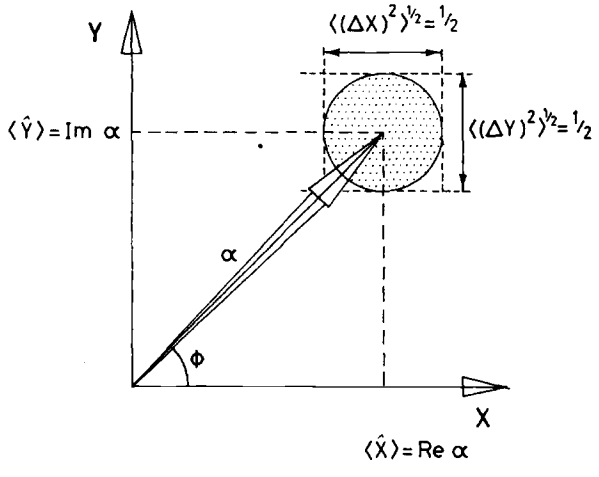

Figure 3. Phase-space description of the mean values and uncertainties of the quadrature operators $\hat{X}$ and $\hat{Y}$ for a coherent state.

In terms of the error contours of the phase-space description of the field, the $\hat{D}(\alpha)$ operator translates the vacuum error contour centred at the origin $(0,0)$ to the position $(\mathrm{Re}\,\alpha, \mathrm{Im}\,\alpha)$, whilst leaving the shape and especially the widths $\langle(\Delta X)^2\rangle^{1/2}$ and $\langle(\Delta Y)^2\rangle^{1/2}$ unchanged from the vacuum values. In this way, the coherent state may be regarded as a classical state with added vacuum-fluctuation noise.

2.3. *Optical correlation functions*

The intensity fluctuations of the optical field are described by the Glauber correlation function $G^{(2)}$. The quantum degree of second-order coherence is a measure of the correlation of light intensities at two space-time points, and is evaluated by considering the transition rate for joint absorption (detection) of photons at the two space-time points. We identify the positive-frequency part of the field $\hat{E}^+$ as

$$\hat{E}^+(t) = \tfrac{1}{2}\mathscr{E}_c \hat{a} \exp(-\mathrm{i}\omega t) \tag{2.37}$$

with the negative-frequency part of the field $\hat{E}^- = (\hat{E}^+)^\dagger$. If purely temporal correlations are of interest, we need to compute the field correlations at times t and a later time $t+\tau$ measured at the same space point. The relevant correlation function is

$$G^{(2)}(t, t+\tau) = \langle \hat{E}^-(t)\hat{E}^-(t+\tau)\hat{E}^+(t+\tau)\hat{E}^+(t)\rangle \tag{2.38}$$

or in normalized form

$$g^{(2)}(t, t+\tau) = \frac{\langle \hat{E}^-(t)\hat{E}^-(t+\tau)\hat{E}^+(t+\tau)\hat{E}^+(t)\rangle}{\langle \hat{E}^-(t)\hat{E}^+(t)\rangle^2}. \tag{2.39}$$

In terms of the normally ordered (dots : denote normal ordering) intensity correlations,

$$g^{(2)}(t, t+\tau) = \frac{\langle : \hat{I}(t+\tau)\hat{I}(t) : \rangle}{\langle \hat{I}(t)\rangle^2}. \tag{2.40}$$

The angle brackets denote quantum expectation values, so that

$$\langle \hat{O}\rangle = \mathrm{Tr}\{\hat{\rho}\hat{O}\}, \tag{2.41}$$

where $\hat{\rho}$ is the field density operator and $\hat{O}$ the operator representing the observable of interest.

For a single-mode radiation field

$$g^{(2)}(t, t) \equiv g^{(2)}(0) = \frac{\langle \hat{a}^\dagger \hat{a}^\dagger \hat{a}\hat{a}\rangle}{\langle \hat{a}^\dagger \hat{a}\rangle^2}, \tag{2.42}$$

so that

$$g^{(2)}(0) - 1 = [\langle(\Delta n)^2\rangle - \langle \hat{n}\rangle]/\langle \hat{n}\rangle^2. \tag{2.43}$$

The photon number variance $\langle(\Delta n)^2\rangle$ is also described by Mandel's Q-parameter [22]

$$Q = \frac{\langle(\Delta n)^2\rangle - \langle \hat{n}\rangle}{\langle \hat{n}\rangle} = \langle \hat{n}\rangle[g^{(2)}(0) - 1]. \tag{2.44}$$

If the single-mode field is prepared in a coherent state, the photon number uncertainty is

$$\langle(\Delta n)_\alpha^2\rangle = \langle\hat{n}\rangle \tag{2.45}$$

and

$$g^{(2)}(0) - 1 = 0. \tag{2.46}$$

The uncertainties in the field photon number and phase for a strong coherent state ($|\alpha| \gg 1$) can be deduced geometrically from the pictorial representation of the coherent state given in figure 3. The field strength is uncertain by an amount given by the *radius* of the uncertainty 'circle', i.e. by $\frac{1}{4}$, so that the photon number uncertainty is given by

$$(|\alpha| \pm \tfrac{1}{4})^2 \approx |\alpha|^2 \pm \tfrac{1}{2}|\alpha| = \langle\hat{n}\rangle \pm \tfrac{1}{2}\langle(\Delta n)^2\rangle^{1/2}. \tag{2.47}$$

Hence

$$\langle(\Delta n)^2\rangle^{1/2} = |\alpha| \tag{2.48}$$

as in equation (2.17). The phase uncertainty is given by the angle subtended at the origin by the uncertainty circle, which is

$$\Delta\phi = 1/2|\alpha|, \tag{2.49}$$

so that the coherent state satisfied the semiclassical number–phase equality

$$\langle(\Delta n)^2\rangle^{1/2}\Delta\phi = 1/2. \tag{2.50}$$

2.4. *Quantum quasiprobability functions*

The density operator may be represented in a diagonal coherent-state, or P-representation [20, 23], according to

$$\hat{\rho} = \int P(\alpha)|\alpha\rangle\langle\alpha|\, \mathrm{d}^2\alpha, \tag{2.51}$$

where $\mathrm{d}^2\alpha \equiv \mathrm{d}(\mathrm{Re}\,\alpha)\,\mathrm{d}(\mathrm{Im}\,\alpha)$ and $P(\alpha)$ is the coherent-state quasiprobability (which need not be positive definite). If we find a state of the field for which $g^{(2)}(0) - 1 > 0$, the field is said to be bunched, with super-Poissonian field statistics, whereas if $g^{(2)}(0) - 1 < 0$, the field is said to be antibunched, with sub-Poissonian field statistics. In general we may write the intensity correlation function using the P-representation equation (2.51) as

$$g^{(2)}(0) - 1 = \frac{\int P(\alpha)[|\alpha|^2 - \langle|\alpha|^2\rangle]^2\, \mathrm{d}^2\alpha}{\left[\int P(\alpha)|\alpha|^2\, \mathrm{d}^2\alpha\right]^2}, \tag{2.52}$$

where $\langle|\alpha|^2\rangle = \int P(\alpha)|\alpha|^2\, \mathrm{d}^2\alpha$.

In terms of the coherent-state representation, the quadrature operator variances are

$$\langle(\Delta X)^2\rangle = \frac{1}{4}\left\{1 + \int P(\alpha)[(\alpha + \alpha^*) - (\langle\alpha\rangle + \langle\alpha^*\rangle)]^2\, \mathrm{d}^2\alpha\right\} \tag{2.53}$$

and

$$\langle(\Delta Y)^2\rangle=\frac{1}{4}\left\{1+\int P(\alpha)[(\alpha-\alpha^*)/\mathrm{i}-(\langle\alpha\rangle-\langle\alpha^*\rangle)/\mathrm{i}]^2\,\mathrm{d}^2\alpha\right\}. \tag{2.54}$$

One immediate consequence of equations (2.52)–(2.54) is that whenever quantum effects are significant (e.g. photon antibunching or a squeezed variance in the quadrature operators below the vacuum limit of $\frac{1}{4}$) the diagonal coherent-state P-function must be *negative* over some range of its argument α. Indeed some authors [1, 24, 25] have used the lack of positivity of the P-function as a signature of quantum effects. Other quantum distribution functions including the Wigner function [26], the positive Drummond–Gardiner complex-P function [27], and the Q-function [2] (defined as the coherent-state expectation value of the density matrix) have been employed in the study of non-classical optical effects such as squeezing. Yuen [12] has derived an expression for the Q-function for a squeezed state, which when plotted as a function of the amplitudes of the two quadratures X and Y produces a graphical realization of the unequal variances in X and Y. Milburn and Walls [28] have studied the effects of dissipative interactions with a reservoir on an initially squeezed state using a Fokker–Planck equation for the Q-function. They show how the squeezed variances relax to their unsqueezed vacuum limits at a rate determined by the damping of the squeezed-mode energy into the reservoir [29].

2.5. *Squeezed states*

So far we have discussed minimum-uncertainty states for which the two quadrature uncertainties are equal. A generalized state, the squeezed state, can remain a minimum-uncertainty state if one variance is compressed at the expense of an expansion of the complementary variance. The modified variances are conveniently written

$$\langle(\Delta X)^2\rangle=\tfrac{1}{4}\exp(-2s), \tag{2.55}$$

$$\langle(\Delta Y)^2\rangle=\tfrac{1}{4}\exp(2s). \tag{2.56}$$

When the squeezing parameter $s=0$, these give the results (2.30) for the vacuum or coherent state, with phase-insensitive equal variances. The squeezing transformation can be written

$$\left.\begin{aligned}\hat{X}\rightarrow\hat{X}_s&=\hat{X}\exp(-s),\\ \hat{Y}\rightarrow\hat{Y}_s&=\hat{Y}\exp(s),\end{aligned}\right\} \tag{2.57}$$

and the corresponding annihilation and creation operators obtained with the use of equations (2.25) and (2.26) are

$$\left.\begin{aligned}\hat{a}_s&=\hat{a}\cosh s-\hat{a}^\dagger\sinh s,\\ \hat{a}_s^\dagger&=\hat{a}^\dagger\cosh s-\hat{a}\sinh s.\end{aligned}\right\} \tag{2.58}$$

These new operators preserve the commutation relations

$$[\hat{X}_s,\hat{Y}_s]=\tfrac{1}{2}\mathrm{i}\quad\text{and}\quad[\hat{a}_s,\hat{a}_s^\dagger]=1. \tag{2.59}$$

The transformed Hamiltonian is

$$\hat{H}=\hbar\omega(\hat{a}_s^\dagger\hat{a}_s+\tfrac{1}{2}) \tag{2.60}$$

with pseudo number states $|n_s\rangle$.

Transformed coherent states may be defined analogously to equations (2.32) and (2.33) through the action of a transformed Glauber displacement operator

$$|\alpha_s\rangle = \hat{D}_s(\alpha)|0_s\rangle \tag{2.61}$$

with

$$\hat{D}_s(\alpha) = \exp(\alpha \hat{a}_s^\dagger - \alpha^* \hat{a}_s). \tag{2.62}$$

The displacement operator transforms the quadrature operators similarly to equation (2.36),

$$\left.\begin{aligned} \hat{X}_s &\to \hat{X}_s + \operatorname{Re}\alpha, \\ \hat{Y}_s &\to \hat{Y}_s + \operatorname{Im}\alpha. \end{aligned}\right\} \tag{2.63}$$

The error contour in $\hat{X}_s$, $\hat{Y}_s$ space remains circular since the state defined in equation (2.61) is a true coherent state in this space. However, in the original $\hat{X}$, $\hat{Y}$ space, the exponentials in equations (2.55) and (2.56) for $s>0$ compress the $\hat{X}$ variance and expand the $\hat{Y}$ variance to produce an elliptical error contour. The squeezing condition for the $\hat{X}$ quadrature is that its variance should be less than the vacuum value,

$$\langle(\Delta X)^2\rangle < \tfrac{1}{4}. \tag{2.64}$$

The state $|0_s\rangle$ represents the squeezed vacuum state.

So far we have considered squeezing of a special kind in which the compression and expansion of the canonical variables are oriented parallel to the $\hat{X}$ and $\hat{Y}$ axes respectively. A more general quadratic generator of squeezed states is given by the unitary squeeze operator [8–14],

$$\hat{S}(\zeta) = \exp(\tfrac{1}{2}\zeta^* \hat{a}^2 - \tfrac{1}{2}\zeta \hat{a}^{\dagger 2}), \tag{2.65}$$

where ζ is the complex squeeze parameter

$$\zeta = s\exp(i\theta), \quad 0 \leqslant s < \infty, \quad 0 \leqslant \theta \leqslant 2\pi. \tag{2.66}$$

This more general transformation corresponds to compression and expansion of the canonical variables in directions inclined at angles $\theta/2$ to the $\hat{X}$ and $\hat{Y}$ axes. The coherent-state error circle shown in figure 3 is now deformed into the squeezed-state error ellipse shown in figure 4. The squeeze operator transforms the annihilation and creation operators as

$$\left.\begin{aligned} \hat{a} &\to \hat{S}^{-1}(\zeta)\hat{a}\hat{S}(\zeta) = \hat{a}\cosh s - \hat{a}^\dagger \exp(i\theta)\sinh s, \\ \hat{a}^\dagger &\to \hat{S}^{-1}(\zeta)\hat{a}^\dagger\hat{S}(\zeta) = \hat{a}^\dagger \cosh s - \hat{a}\exp(-i\theta)\sinh s. \end{aligned}\right\} \tag{2.67}$$

If $\theta = 0$, these reduce to the relations (2.58) produced by the transformation (2.57). The more detailed variance properties of the squeezed states with $\theta \neq 0$ are discussed in § 3.2.

When we come to consider the problem of the detection of squeezed light in § 5.2, we will find that the measured signal is determined by the electric-field operator (2.27) except that the factor ωt is replaced by a field phase angle χ governed by the properties of the detector. We define the phase-angle-dependent electric field $\hat{E}(\chi)$ by

$$\hat{E}(\chi) = \tfrac{1}{2}\mathscr{E}_c\{\exp(i\chi)\hat{a}^\dagger + \exp(-i\chi)\hat{a}\}. \tag{2.68}$$

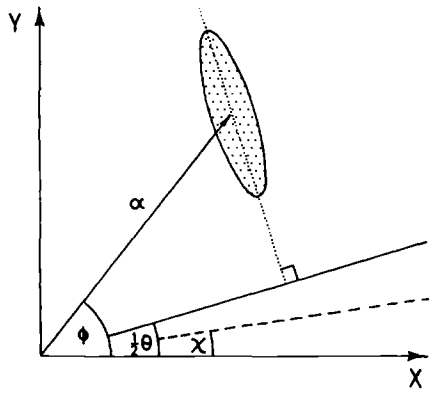

Figure 4. Phase-space description of the mean values and uncertainties of the quadrature operators $\hat{X}$ and $\hat{Y}$ for a squeezed state. The angle χ is the homodyne phase-detection angle.

The direction of this complex vector is represented by the dashed line in figure 4. The mean and the variance of the detected signal are given by the projections of the complex amplitude vector α and the uncertainty ellipse onto this line which represents $\hat{E}(\chi)$ in units of $\mathscr{E}_c$. The corresponding operators at phase angles zero and χ have the commutation relation

$$[\hat{E}(0), \hat{E}(\chi)] = \tfrac{1}{2}i\mathscr{E}_c^2 \sin\chi, \tag{2.69}$$

and associated uncertainty relation

$$\langle(\Delta E(0))^2\rangle^{1/2}\langle(\Delta E(\chi))^2\rangle^{1/2} \geqslant \tfrac{1}{4}\mathscr{E}_c^2|\sin\chi|. \tag{2.70}$$

For a coherent state, the electric-field variance is given by

$$\langle(\Delta E(\chi))_\alpha^2\rangle = (\tfrac{1}{2}\mathscr{E}_c)^2, \tag{2.71}$$

independent of phase angle χ. This satisfies equation (2.70) as an equality, where of course $|\sin\chi|$ must in this case take its maximum value. This reflects the phase-independent quantum noise of a coherent field. For some values of phase angle χ for a squeezed state, this variance is less than that of the coherent field,

$$\langle(\Delta E(\chi))^2\rangle < (\tfrac{1}{2}\mathscr{E}_c)^2. \tag{2.72}$$

It is of interest to study the wavepacket dynamics of a squeezed state of a material oscillator of unit mass. As we saw earlier in equations (2.23) and (2.24) a coherent-state wavepacket oscillates to and fro whilst preserving its initial width. Sargent, Scully and Lamb [18] discuss the general evolution of a Gaussian wavepacket. They find that its centre executes simple harmonic motion but with a width that varies in time as

$$\langle(\Delta q)^2\rangle = (\cos^2\omega t + R^2\sin^2\omega t)/R, \tag{2.73}$$

where R plays the role of our squeeze parameter. Takahasi [6], Nieto [30] and Stenholm [31, 32] have further studied the wavepacket dynamics of squeezed states.

3. Minimum-uncertainty squeezed states

The squeezed states defined in § 2.5 are important not only for their theoretical interest as minimum-uncertainty states but also for their practical realizability in four-wave mixing and parametric-generation experiments performed under optimum conditions (see § 6). In the present section we discuss the detailed properties of these single-mode squeezed states and outline their generalization to states that involve excitation of larger numbers of modes.

3.1. *Alternative definitions*

There are two equivalent but different definitions and notations in common usage, and we first clarify the relations between them. The 'ideal squeezed states' of Caves [14] are defined to be

$$|\alpha, \zeta\rangle = \hat{D}(\alpha)\hat{S}(\zeta)|0\rangle, \tag{3.1}$$

where $\hat{D}(\alpha)$ is the coherent displacement operator of equation (2.33), $\hat{S}(\zeta)$ is the unitary squeeze operator of equation (2.65) and $|0\rangle$ is the single-mode vacuum state. An important special case of equation (3.1) is the definition of the squeezed vacuum state, which appears on the right-hand side of equation (2.61), and which now takes the form

$$|0, \zeta\rangle \equiv |0_s\rangle = \hat{S}(\zeta)|0\rangle. \tag{3.2}$$

A geometrical representation of the definition (3.1) is shown in figure 5 (*a*), with a first step in which the single-mode vacuum is squeezed, converting its uncertainty circle to an ellipse, and a second step in which the centre of the ellipse is translated from the origin to the coherent complex amplitude α.

In the earlier work of Yuen [12] on the equivalent 'two-photon coherent states', the corresponding definition is written

$$|\beta; \mu, \nu\rangle = \hat{U}_L\hat{D}(\beta)|0\rangle, \tag{3.3}$$

where $\hat{U}_L$ is the squeeze operator, equivalent to $\hat{S}(\zeta)$ in equation (2.65), and the coherent displacement operator is defined in (2.33). The Yuen squeezed-state parameters are related to the Caves notation by

$$\left.\begin{aligned} \beta &= \mu\alpha + \nu\alpha^*, \\ \mu &= \cosh s, \\ \nu &= \exp(i\theta)\sinh s. \end{aligned}\right\} \tag{3.4}$$

A geometrical representation of the definition (3.3) is shown in figure 5 (*b*), with a first step in which the centre of the vacuum-state uncertainty circle is translated from the origin to the coherent complex amplitude β, and a second step in which the squeeze operator converts the circle to an uncertainty ellipse and produces a further translation of its centre from β to α. Thus the squeeze operator in (3.3) acts on the amplitude vector of the coherent state $|\beta\rangle$ as well as its uncertainty distribution, but the relations (3.4) between the parameters in the two definitions ensure that the squeezed states (3.1) and (3.3) are identical.

The Caves and the Yuen notations for squeezed states can be used interchangably: one or the other may be particularly convenient for a specific calculation. The discussion that follows uses only the Caves notation, to avoid confusion, but it should

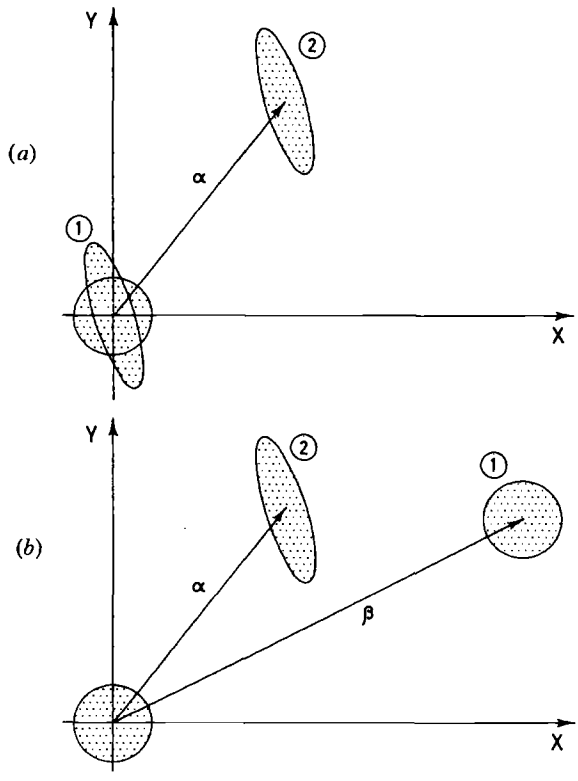

Figure 5. Geometrical representations of the definitions of the ideal squeezed state according to the prescriptions of (*a*) Caves and (*b*) Yuen.

be emphasized that the Yuen paper [12] is the original source for many of the more important properties of the ideal squeezed states. One of these is the form of eigenvalue equation satisfied by the states, which can be derived from equations (2.32), (2.34), (2.67) and (3.1) as

$$(\hat{a}\cosh s+\hat{a}^{\dagger}\exp(\mathrm{i}\theta)\sinh s)|\alpha,\zeta\rangle=(\alpha\cosh s+\alpha^{*}\exp(\mathrm{i}\theta)\sinh s)|\alpha,\zeta\rangle. \tag{3.5}$$

This form of the eigenvalue equation is closely related to the minimum-uncertainty properties of the squeezed states discussed in § 3.2 below.

3.2. *Quadrature uncertainties*

Squeezed-state expectation values, denoted by simple angle brackets, can be obtained from the definition (3.1) with the use of the transformation properties (2.34) and (2.67). Thus

$$\langle\hat{a}\rangle=\alpha \quad \text{and} \quad \langle\hat{a}^{\dagger}\rangle=\alpha^{*}, \tag{3.6}$$

being independent of the squeeze parameters. The mean photon number is

$$\langle\hat{n}\rangle=\langle\hat{a}^{\dagger}\hat{a}\rangle=|\alpha|^{2}+\sinh^{2}s; \tag{3.7}$$

the first contribution on the right is associated with the coherent amplitude α, while

the second contribution arises from the squeezing of the vacuum. The same identification applies to the two contributions in the expectation value

$$\langle \hat{a}\hat{a} \rangle = \alpha^2 - \exp(i\theta) \sinh s \cosh s. \tag{3.8}$$

These results provide the means and variances of the quadrature operators defined in equations (2.25) and (2.26) as

$$\left.\begin{aligned} \langle \hat{X} \rangle &= \tfrac{1}{2}(\alpha + \alpha^*) = \operatorname{Re} \alpha, \\ \langle \hat{Y} \rangle &= \frac{1}{2i}(\alpha - \alpha^*) = \operatorname{Im} \alpha, \end{aligned}\right\} \tag{3.9}$$

and

$$\left.\begin{aligned} \langle (\Delta X)^2 \rangle &= \tfrac{1}{4}\{\exp(-2s) \cos^2 \tfrac{1}{2}\theta + \exp(2s) \sin^2 \tfrac{1}{2}\theta\}, \\ \langle (\Delta Y)^2 \rangle &= \tfrac{1}{4}\{\exp(-2s) \sin^2 \tfrac{1}{2}\theta + \exp(2s) \cos^2 \tfrac{1}{2}\theta\}. \end{aligned}\right\} \tag{3.10}$$

The variances are independent of the coherent amplitude α and they can be represented pictorially by the uncertainty ellipses shown in some of the above figures. These ellipses can be defined in terms of contours of the squeezed-state Wigner function [12], but we use here a simple definition that is illustrated in figure 6. With an ellipse having the sizes and orientations of major and minor axes shown, a simple application of elliptical theory shows that the projections of the ellipse on to the X and Y axes are equal to the square roots of the corresponding variances. The complete pictorial representation shown in figure 4 thus correctly reproduces the mean and variance expressions (3.9) and (3.10).

The squeezing condition (2.64) for the quadrature operator $\hat{X}$ is satisfied by (3.10) if [33]

$$\cos \theta > \tanh s, \tag{3.11}$$

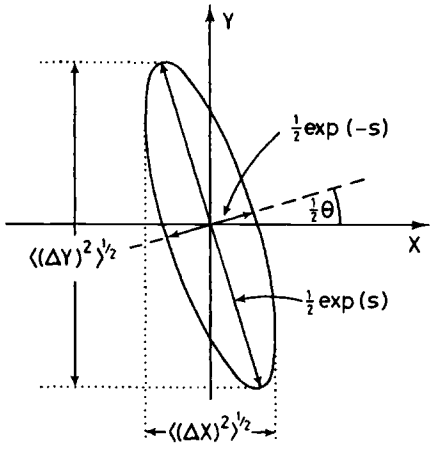

Figure 6. Uncertainty ellipse of the ideal squeezed vacuum state showing how s and θ determine the axis lengths and orientation, and with the quadrature operator variances obtained from projections on to the X and Y axes.

and the minimum value is

$$\langle(\Delta X)^2\rangle=\tfrac{1}{4}\exp(-2s) \quad \text{for} \quad \theta=0, \tag{3.12}$$

in agreement with equation (2.55). The restriction (3.11) on θ becomes more severe for the more highly squeezed states. The squeezing condition is equivalent to that for a negative normally ordered variance; the normally ordered variances are obtained from the expressions in (3.10) by subtraction of $\frac{1}{4}$. The squeezing condition for the quadrature operator $\hat{Y}$ is satisfied if

$$\cos\theta<-\tanh s. \tag{3.13}$$

The uncertainty product obtained from the variances (3.10) is

$$\langle(\Delta X)^2\rangle^{1/2}\langle(\Delta Y)^2\rangle^{1/2}=\tfrac{1}{4}\{\cosh^2 2s\sin^2\theta+\cos^2\theta\}^{1/2}. \tag{3.14}$$

This takes the minimum-uncertainty-state value

$$\langle(\Delta X)^2\rangle^{1/2}\langle(\Delta Y)^2\rangle^{1/2}=\tfrac{1}{4} \quad \text{for} \quad \theta=0 \text{ or } \pi, \tag{3.15}$$

but is larger for other angles, with a maximum value

$$\langle(\Delta X)^2\rangle^{1/2}\langle(\Delta Y)^2\rangle^{1/2}=\tfrac{1}{4}\cosh 2s \quad \text{for} \quad \theta=\tfrac{1}{2}\pi \text{ or } \tfrac{3}{2}\pi. \tag{3.16}$$

Note however that, as is clear from the pictorial representation in figure 6, the squeezed state (3.1) defined for an arbitrary value of θ is a minimum-uncertainty state for a new pair of quadrature operators corresponding to directions inclined at angles $\frac{1}{2}\theta$ to the X and Y axes. This property is ensured by the form of the eigenvalue equation (3.5).

The ideal squeezed state (3.1) is converted to the ordinary coherent state $|\alpha\rangle$ on setting ζ equal to zero, and all of the above expressions simplify to their coherent-state counterparts when s is put equal to zero. In the opposite extreme of very large s, the uncertainty ellipse is flattened to approach the form of a line oriented perpendicular to the direction $\frac{1}{2}\theta$ in the XY-plane. Thus for $\theta=0$, as in (3.12) the X-coordinate uncertainty tends to zero for $s\to\infty$ [34], but the Y uncertainty diverges exponentially. These can be designated 'line' states, and the $\theta=0$ line state is an eigenfunction $|X\rangle$ of the operator $\hat{X}$,

$$\hat{X}|X\rangle=X|X\rangle. \tag{3.17}$$

A coordinate representation, or wavefunction, of the squeezed state $|\alpha,s\rangle$ can be defined in terms of its projection on to the line state $|X\rangle$, given by [12]

$$\langle X|\alpha,s\rangle=[2\exp(2s)/\pi]^{1/4}\exp\{-(x-\operatorname{Re}\alpha)^2\exp(2s)+2ix\operatorname{Im}\alpha-i\operatorname{Re}\alpha\operatorname{Im}\alpha\}, \tag{3.18}$$

for $\theta=0$. Thus

$$|\langle X|\alpha,s\rangle|^2=[2\exp(2s)/\pi]^{1/2}\exp[-2(x-\operatorname{Re}\alpha)^2\exp(2s)], \tag{3.19}$$

showing that the squeezed state has the form of a Gaussian wavepacket as discussed in § 2.

3.3. *Number and phase uncertainties*

The photon-number mean value for the ideal squeezed state is given in (3.7). The photon-number variance is obtained straightforwardly by a similar calculation, in the form

$$\langle(\Delta n)^2\rangle = |\alpha|^2[\exp(-2s)\cos^2(\phi-\tfrac{1}{2}\theta)+\exp(2s)\sin^2(\phi-\tfrac{1}{2}\theta)]+2\sinh^2 s\cosh^2 s, \tag{3.20}$$

where $\alpha=|\alpha|\exp(i\phi)$. The expressions (3.7) and (3.20) can be used to obtain explicit results for the degree of second-order coherence defined in equation (2.43) and Mandel's Q-parameter defined in equation (2.44). We do not write down the general results but consider two limiting cases of practical importance.

The practical sources of squeezed light described in § 6.6 commonly generate the squeezed vacuum state, where $\alpha=0$, and (3.7) and (3.20) give

$$\langle(\Delta n)^2\rangle = 2\langle\hat{n}\rangle(\langle\hat{n}\rangle+1). \tag{3.21}$$

The definitions (2.43) and (2.44) therefore give

$$g^{(2)}(0)=3+(1/\langle\hat{n}\rangle) \tag{3.22}$$

and

$$Q=2\langle\hat{n}\rangle+1. \tag{3.23}$$

The squeezed vacuum-state light thus shows photon bunching and super-Poissonian statistics.

Although the above characteristics typify the light output from the source, the homodyne detection technique used to evaluate the amount of squeezing in a light beam, which is described in detail in § 5.2, has the effect of adding a large coherent component to the received light. The light that is ultimately detected thus has the form of a squeezed state in which the coherent contribution to the mean photon number, given by the first term in (3.7), greatly exceeds the squeezing contribution, given by the second term. We therefore consider the limit

$$|\alpha|^2 \gg \exp(2s), \quad \langle n\rangle \approx |\alpha|^2, \tag{3.24}$$

where (3.20) can be approximated by

$$\langle(\Delta n)^2\rangle = |\alpha|^2[\exp(-2s)\cos^2(\phi-\tfrac{1}{2}\theta)+\exp(2s)\sin^2(\phi-\tfrac{1}{2}\theta)]. \tag{3.25}$$

Note that this expression is obtained for the uncertainty in the square of the coherent amplitude, if the uncertainty in the amplitude itself is represented geometrically by the projection of the ellipse in figure 4 on to the amplitude vector, in a calculation similar to that of equation (2.47). The Q-parameter and degree of second-order coherence given by equation (2.44) in the same limit (3.24) are obtained from

$$\begin{aligned} Q &= [\exp(-2s)-1]\cos^2(\phi-\tfrac{1}{2}\theta)+[\exp(2s)-1]\sin^2(\phi-\tfrac{1}{2}\theta) \\ &= |\alpha|^2(g^{(2)}-1). \end{aligned} \tag{3.26}$$

Photon antibunching and sub-Poissonian photon statistics therefore occur if

$$\cos(2\phi-\theta) > \tanh s, \tag{3.27}$$

and by comparison with (3.11) this is seen to be the same as the condition for squeezing in the direction parallel to the coherent amplitude vector α. The addition

of a large coherent amplitude can thus convert the super-Poissonian statistics of the squeezed vacuum state, represented by (3.22) and (3.23), into photon number distributions that show non-classical properties. For a given value of s, the extremal values are

$$Q_{\min}=|\alpha|^2(g^{(2)}-1)_{\min}=\exp(-2s)-1 \quad \text{for} \quad \phi=\tfrac{1}{2}\theta \tag{3.28}$$

and

$$Q_{\max}=|\alpha|^2(g^{(2)}-1)_{\max}=\exp(2s)-1 \quad \text{for} \quad \phi=\tfrac{1}{2}\theta+\tfrac{1}{2}\pi. \tag{3.29}$$

The photon number mean and variance are properties of the complete ideal-squeezed-state photon number distribution, which can be written in the form

$$P_n=|\langle n|\alpha,\zeta\rangle|^2, \tag{3.30}$$

where [12]

$$\langle n|\alpha,\zeta\rangle=(n!\cosh s)^{-1/2}[\tfrac{1}{2}\exp(\mathrm{i}\theta)\tanh s]^{n/2}$$
$$\times\exp\{-\tfrac{1}{2}[|\alpha|^2+\alpha^*\exp(\mathrm{i}\theta)\tanh s]\}H_n\left\{\frac{\alpha+\alpha^*\exp(\mathrm{i}\theta)\tanh s}{(2\exp(\mathrm{i}\theta)\tanh s)^{1/2}}\right\}, \tag{3.31}$$

where H_n is the Hermite polynomial of degree n. This complicated expression simplifies considerably in the limit (3.24) of a strong coherent component, when the photon number distribution is given approximately by the Gaussian expression

$$P_n=\exp[-(n-|\alpha|^2)^2/2\langle(\Delta n)^2\rangle]/(2\pi\langle(\Delta n)^2\rangle)^{1/2}, \tag{3.32}$$

where the variance is given by (3.25). Figures 7 and 8 show some graphs of the exact and asymptotic photon-number distributions for the angular conditions assumed in (3.28) and (3.29), together with the coherent-state Poisson distribution to which (3.30) reduces for $s=0$.

The phase-angle uncertainty of the ideal squeezed state can be calculated by the phase operator methods familiar in the treatment of the coherent state [35]. We again consider only the limit (3.24) where the coherent contribution to the mean photon number greatly exceeds the squeezing contribution. The phase-angle uncertainty is

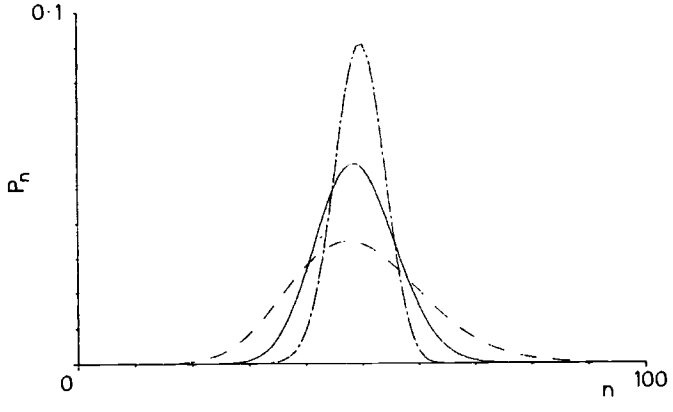

Figure 7. Photon number distributions P_n computed from exact formulae equations (3.30) and (3.31) for $|\alpha|^2=49$ for coherent light (solid line) with $s=0$, and squeezed light with $s=0{\cdot}5$, $\phi=\theta/2$ (the dash-dot line) and with $s=0{\cdot}5$, $\phi=\theta/2+\pi/2$ (the dashed line). The Mandel Q parameter is zero, $(1/e)-1$ and $e-1$, respectively.

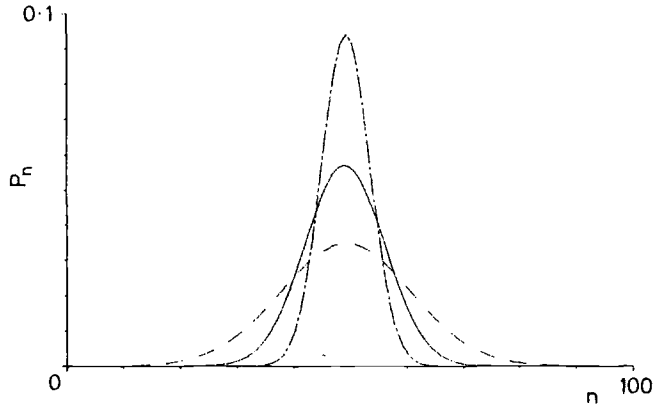

Figure 8. Photon number distributions P_n as in figure 7 but calculated from the asymptotic form given in equation (3.32).

then obtained from a calculation similar to that in equation (2.49) as the angle subtended by the uncertainty ellipse at the origin, with an arc length given by the projection of the ellipse on the direction perpendicular to the coherent vector. Thus

$$(\Delta\phi)^2 = [\exp(-2s)\sin^2(\phi - \tfrac{1}{2}\theta) + \exp(2s)\cos^2(\phi - \tfrac{1}{2}\theta)\}/4|\alpha|^2. \tag{3.33}$$

It is seen from (3.25) and (3.33) that

$$\langle(\Delta n)^2\rangle^{1/2}\Delta\phi = \tfrac{1}{2} \quad \text{for} \quad \phi = \tfrac{1}{2}\theta \quad \text{and} \quad \phi = \tfrac{1}{2}\theta + \tfrac{1}{2}\pi, \tag{3.34}$$

in agreement with the minimum-uncertainty relation (2.50), but the uncertainty product is larger for other angles. Note that the angles for minimum number-phase uncertainty differ from the angles for minimum quadrature-operator uncertainty given in (3.15).

3.4. *Multimode squeezed states*

Several of the experimental methods of squeezed-state generation described in § 6.6 produce output light at two distinct frequencies, denoted here ω_+ and ω_-. The resulting excitation may be described as a two-mode squeezed state defined by [36, 37]

$$|\alpha_+, \alpha_-, \zeta\rangle = \hat{D}_+(\alpha_+)\hat{D}_-(\alpha_-)\hat{S}_{+-}(\zeta)|0\rangle, \tag{3.35}$$

where

$$\hat{D}_\pm(\alpha_\pm) = \exp(\alpha_\pm \hat{a}_\pm^\dagger - \alpha_\pm^* \hat{a}_\pm) \tag{3.36}$$

is the coherent displacement operator for the two modes described by destruction operators $\hat{a}_+$ and $\hat{a}_-$,

$$\hat{S}_{+-}(\zeta) = \exp(\zeta^* \hat{a}_+ \hat{a}_- - \zeta \hat{a}_+^\dagger \hat{a}_-^\dagger), \tag{3.37}$$

with ζ defined by (2.66), is the unitary two-mode squeeze operator, and $|0\rangle$ is the two-mode vacuum state.

The displacement operators have the property (2.34) for each of the two modes, while the squeezing operator transforms the destruction operators according to

$$\hat{S}_+^{-1}{}_-(\zeta)\hat{a}_\pm\hat{S}_+{}_-(\zeta)=\hat{a}_\pm\cosh s-\hat{a}_\mp^\dagger\exp(\mathrm{i}\theta)\sinh s. \tag{3.38}$$

The use of these properties enables the expectation values of creation and destruction operator combinations for the two-mode squeezed states to be calculated straightforwardly. The lower-order expectation values are

$$\langle\hat{a}_+\rangle=\alpha_+ \quad\text{and}\quad \langle\hat{a}_-\rangle=\alpha_-, \tag{3.39}$$

$$\langle\hat{a}_+^\dagger\hat{a}_+\rangle=|\alpha_+|^2+\sinh^2 s \quad\text{and}\quad \langle\hat{a}_-^\dagger\hat{a}_-\rangle=|\alpha_-|^2+\sinh^2 s, \tag{3.40}$$

$$\langle\hat{a}_+^\dagger\hat{a}_-\rangle=\alpha_+^*\alpha_- \quad\text{and}\quad \langle\hat{a}_-^\dagger\hat{a}_+\rangle=\alpha_-^*\alpha_+, \tag{3.41}$$

$$\langle\hat{a}_+\hat{a}_+\rangle=\alpha_+^2 \quad\text{and}\quad \langle\hat{a}_-\hat{a}_-\rangle=\alpha_-^2 \tag{3.42}$$

$$\langle\hat{a}_+\hat{a}_-\rangle=\langle\hat{a}_-\hat{a}_+\rangle=\alpha_+\alpha_--\exp(\mathrm{i}\theta)\sinh s\cosh s. \tag{3.43}$$

It is seen by comparison with the single-mode results (3.7) and (3.8) that the squeezing affects only the diagonal photon-number expectation values (3.40) for each individual mode and the off-diagonal intermode expectation values (3.43).

The quadrature operator $\hat{X}$ of equation (2.25) is generalized in the two-mode case to

$$\hat{X}=(\hat{a}_++\hat{a}_+^\dagger+\hat{a}_-+\hat{a}_-^\dagger)/2^{3/2}. \tag{3.44}$$

It is not difficult to verify with the use of (3.39) to (3.43) that the mean and variance are

$$\langle X\rangle=(\mathrm{Re}\,\alpha_++\mathrm{Re}\,\alpha_-)/2^{1/2} \tag{3.45}$$

and

$$\langle(\Delta X)^2\rangle=\tfrac{1}{4}[\exp(-2s)\cos^2\tfrac{1}{2}\theta+\exp(2s)\sin^2\tfrac{1}{2}\theta]. \tag{3.46}$$

These results are to be compared with (3.9) and (3.10) for the single-mode case, and it is seen that the variances are identical. Appropriate measurements for the single-mode and two-mode squeezed states can thus produce very similar readings, with variances that may lie below the value of $\frac{1}{4}$ associated with the ordinary coherent state. The natures of the required measurements are described in § 5.4.

All of the above discussion of squeezed states has treated the field excitations in terms of one or two discrete modes. In practice, sources of squeezed light radiate into free space, where there is a continuous distribution of field modes. The emitted light generally excites a spread of frequencies, and the single- and two-mode excitations are replaced by continuous-frequency distributions with one or two spectral peaks. It is more natural in free space to work with photon flux operators rather than photon number operators. Spectral distributions of squeezed light have been calculated for various kinds of source [38]. The parametric amplifier in a cavity is a particularly important example since it can ideally produce squeezed light with characteristics akin to the single- and two-mode varieties discussed above, when operated in a degenerate and a non-degenerate manner respectively [39, 40]. The continuous-mode theory [41] shows that for detection schemes in which the measurement selects only frequencies close to the degenerate frequency ω, or the non-degenerate frequencies ω_+ and ω_-, with a bandwidth that is small compared with the spectral width of the emission, the predicted outcomes are identical with those that result

from the discrete-mode theories outlined above. For broader bandwidth measurements, it is necessary to take account of the detailed spectral distribution of the squeezed light.

4. Atomic sources of squeezing

4.1. *Squeezing in resonance fluorescence from two-level atoms*

Resonance fluorescence from a single two-level atom is known to exhibit nonclassical field fluctuations which are responsible for the triplet spectrum of emitted light from atoms resonantly excited by intense fields [42, 43], photon antibunching [44–48] and sub-Poissonian photon statistics [49]. Walls and Zoller [50] predicted that squeezing is present both in the dipole operator variables and in the multimode fluorescent light. The squeezing in the fluorescent field is of a broadband character, reflecting the infinite number of free-space modes involved in the atomic transition.

The atomic response to the incident coherent laser field is described by the two-level optical Bloch equations [19, 51] which govern the evolution of the induced dipole moment and the excited-state population or inversion. We consider a two-level atom with a ground state $|1\rangle$ and an excited state $|2\rangle$ separated by energy $\hbar\omega_0$, interacting with a single-mode beam of light in a coherent state $|\alpha\rangle$ with frequency ω. We describe the atomic transitions in terms of the raising ($\hat{\Pi}^\dagger$) and lowering ($\hat{\Pi}$) operators

$$\left.\begin{aligned}\hat{\Pi}^\dagger &= |2\rangle\langle 1|,\\ \hat{\Pi} &= |1\rangle\langle 2|,\end{aligned}\right\} \tag{4.1}$$

so that the atomic dipole operator $\hat{\mathbf{D}} = \mathbf{D}_{12}(\hat{\Pi}^\dagger + \hat{\Pi})$. Then the Hamiltonian for the coupled atom–field system is

$$\hat{H} = \hbar\omega_0\hat{\Pi}^\dagger\hat{\Pi} + \sum_\lambda \hbar\omega_\lambda \hat{a}_\lambda^\dagger \hat{a}_\lambda + i\sum_\lambda \hbar g_\lambda [\hat{\Pi}^\dagger \hat{a}_\lambda \exp(i\mathbf{k}\cdot\mathbf{R}) - \hat{a}_\lambda^\dagger \hat{\Pi} \exp(-i\mathbf{k}\cdot\mathbf{R})], \tag{4.2}$$

where λ labels the field-mode wave-vector $\mathbf{k}$ and polarization $\boldsymbol{\varepsilon}_\lambda$, and $\mathbf{R}$ is the atomic position. The coupling constant g_λ is given by

$$g_\lambda \equiv e\left(\frac{\omega_\lambda}{2\varepsilon_0 V\hbar}\right)^{1/2} \boldsymbol{\varepsilon}_\lambda \cdot \mathbf{D}_{12}, \tag{4.3}$$

where V is the quantization volume.

We calculate the field and atom dynamics using the Heisenberg picture making the usual Born–Markov approximations for the spontaneously radiated field. The field mode operator at time t is given by the general expression

$$\hat{a}_\lambda(t) = \hat{a}_\lambda(0)\exp(-i\omega_\lambda t) - g_\lambda \int_0^t dt'\, \hat{\Pi}(t')\exp(-i\mathbf{k}\cdot\mathbf{R})\exp[i\omega_\lambda(t'-t)]. \tag{4.4}$$

The total positive-frequency part of the radiated electric field at position $\mathbf{r}$ is given by

$$\hat{\mathbf{E}}^+(\mathbf{r},t) = i\sum_\lambda \left(\frac{\hbar\omega_\lambda}{2\varepsilon_0 V}\right)^{1/2} \boldsymbol{\varepsilon}_\lambda \hat{a}_\lambda(t)\exp(i\mathbf{k}\cdot\mathbf{r}) \tag{4.5}$$

and can be decomposed into a free-field part $\hat{\mathbf{E}}_f^+$ and a source-field part $\hat{\mathbf{E}}_s^+$, given by [19]

$$\hat{\mathbf{E}}_s^+(\mathbf{r},t) = -\mathrm{i}(e/16\pi^3\varepsilon_0)\int \mathrm{d}\mathbf{k}\,\boldsymbol{\varepsilon}_\lambda(\boldsymbol{\varepsilon}_\lambda\cdot\mathbf{D}_{12}) \times \exp[\mathrm{i}\mathbf{k}\cdot(\mathbf{r}-\mathbf{R})-\mathrm{i}\omega_\lambda t]\int_0^t \mathrm{d}t'\,\hat{\Pi}(t')\exp(\mathrm{i}\omega_\lambda t'), \quad (4.6)$$

which on integration becomes

$$\hat{\mathbf{E}}_s^+(\mathbf{r},t) = -\left(\frac{e\omega_0^2 D_{12}\sin\psi}{4\pi\varepsilon_0 c^2|\mathbf{r}-\mathbf{R}|}\right)\hat{\mathbf{i}}\hat{\Pi}(t-|\mathbf{r}-\mathbf{R}|/c)\equiv\mu\hat{\Pi}(t-|\mathbf{r}-\mathbf{R}|/c), \quad (4.7)$$

where ψ is the angle between the dipole moment $\mathbf{D}_{12}$ and $\mathbf{r}$.

We next need to describe the atomic transition dynamics. This is conveniently carried out in the interaction picture using the optical Bloch equations for the atomic density matrix. The interaction-picture Hamiltonian $\hat{H}_I$ is derived from the Schrödinger-picture Hamiltonian (equation (4.2)) by

$$\hat{H}_I = \exp(+\mathrm{i}\hat{H}_0 t/\hbar)\,\hat{H}\exp(-\mathrm{i}\hat{H}_0 t/\hbar)$$

where $\hat{H}_0$ comprises the free-field and unperturbed Hamiltonian

$$\hat{H}_0 = \hbar\omega_0\hat{\Pi}^\dagger\hat{\Pi} + \sum_\lambda \hbar\omega_\lambda \hat{a}_\lambda^\dagger\hat{a}_\lambda \quad (4.8)$$

so that

$$\hat{H}_I(t) = \mathrm{i}\sum_\lambda \hbar g_\lambda\{\hat{\Pi}^\dagger\hat{a}_\lambda\exp[\mathrm{i}(\omega_0-\omega_\lambda)t+\mathrm{i}\mathbf{k}\cdot\mathbf{R}]-\mathrm{h.c.}\}. \quad (4.9)$$

In terms of the density matrix elements ρ_{ij}, the expectation values of the atomic operators are

$$\left.\begin{aligned}\langle\hat{\Pi}(t)\rangle &= \mathrm{Tr}\{\hat{\rho}_I(t)\hat{\Pi}\exp(-\mathrm{i}\omega_0 t)\} = \rho_{21}(t)\exp(-\mathrm{i}\omega_0 t),\\ \langle\hat{\Pi}^\dagger(t)\rangle &= \rho_{12}(t)\exp(\mathrm{i}\omega_0 t),\\ \langle\hat{\Pi}^\dagger(t)\hat{\Pi}(t)\rangle &= \rho_{22}(t).\end{aligned}\right\} \quad (4.10)$$

The optical Bloch equations for an atom driven by an external field in a single-mode coherent state and damped by spontaneous emission at rate γ are

$$\frac{\mathrm{d}}{\mathrm{d}t}\rho_{22} = g\alpha\exp[\mathrm{i}(\omega_0-\omega)t]\,\rho_{12} + g\alpha^*\exp[-\mathrm{i}(\omega_0-\omega)t]\,\rho_{21} - 2\gamma\rho_{22}, \quad (4.11)$$

$$\frac{\mathrm{d}}{\mathrm{d}t}\rho_{12} = g\alpha^*\exp[-\mathrm{i}(\omega_0-\omega)t]\,(\rho_{11}-\rho_{22}) - \gamma\rho_{12}. \quad (4.12)$$

We choose the coherent-state phase ($\alpha = |\alpha|\exp(\mathrm{i}\phi)$) to be $\phi = -\pi/2$, so that $\alpha = -\mathrm{i}|\alpha|$ and define the Rabi frequency Ω by

$$\Omega = 2g|\alpha|. \quad (4.13)$$

The overall oscillatory time dependences in ρ_{12} and ρ_{21} may be factored out by defining the slowly varying quantities

$$\left.\begin{aligned}\bar{\rho}_{12}&=\exp[\mathrm{i}(\omega_0-\omega)t]\rho_{12},\\ \bar{\rho}_{21}&=\exp[-\mathrm{i}(\omega_0-\omega)t]\rho_{21}.\end{aligned}\right\} \tag{4.14}$$

Then in steady-state, we find

$$\rho_{22}=\frac{\frac{1}{4}\Omega^2}{(\omega_0-\omega)^2+\gamma^2+\frac{1}{2}\Omega^2}, \tag{4.15}$$

$$\rho_{12}=-\exp[-\mathrm{i}(\omega_0-\omega)t]\frac{\frac{1}{2}\Omega(\omega_0-\omega-\mathrm{i}\gamma)}{(\omega_0-\omega)^2+\gamma^2+\frac{1}{2}\Omega^2}. \tag{4.16}$$

The uncertainties in the dipole operators can be found easily using equation (4.1). We define quadrature dipole operators $\hat{\Pi}_1$ and $\hat{\Pi}_2$ by analogy with the corresponding quadrature field operators $\hat{X}$, $\hat{Y}$ by

$$\hat{\Pi}^{\dagger}\equiv\hat{\Pi}_1+\mathrm{i}\hat{\Pi}_2, \tag{4.17}$$

$$\hat{\Pi}\equiv\hat{\Pi}_1-\mathrm{i}\hat{\Pi}_2. \tag{4.18}$$

The quadrature dipole operators obey the commutation relation

$$[\hat{\Pi}_1,\hat{\Pi}_2]=\tfrac{1}{2}\mathrm{i}\hat{\Pi}_3, \tag{4.19}$$

where $\hat{\Pi}_3=|2\rangle\langle 2|-|1\rangle\langle 1|$. From equation (4.19) we find the uncertainty relation for the variances

$$\langle(\Delta\Pi_1)^2\rangle\langle(\Delta\Pi_2)^2\rangle\geqslant\frac{1}{16}|\langle\hat{\Pi}_3\rangle|^2, \tag{4.20}$$

and the dipole quadrature $\hat{\Pi}_i$ is said to be squeezed if

$$\langle(\Delta\Pi_i)^2\rangle<\tfrac{1}{4}|\langle\hat{\Pi}_3\rangle|. \tag{4.21}$$

The squares of the operators $\hat{\Pi}_1$ and $\hat{\Pi}_2$ are, using equation (4.1), given by

$$\hat{\Pi}_1^2=\tfrac{1}{4}=\hat{\Pi}_2^2, \tag{4.22}$$

although $\hat{\Pi}_3^2=1$. Therefore

$$\langle(\Delta\Pi_1)^2\rangle=\tfrac{1}{4}-\langle\hat{\Pi}_1\rangle^2 \tag{4.23}$$

with

$$\langle\hat{\Pi}_1\rangle=\tfrac{1}{2}[\bar{\rho}_{12}\exp(\mathrm{i}\omega t)+\bar{\rho}_{21}\exp(-\mathrm{i}\omega t)]. \tag{4.24}$$

We remove the exponential time-dependences of $\langle\hat{\Pi}_1\rangle$ by defining

$$\hat{\sigma}_1=\tfrac{1}{2}[\hat{\Pi}^{\dagger}\exp(-\mathrm{i}\omega t)+\hat{\Pi}\exp(\mathrm{i}\omega t)] \tag{4.25}$$

by analogy with $\hat{E}_1\equiv\frac{1}{2}[\hat{E}^{+}\exp(\mathrm{i}\omega t)+\hat{E}^{-}\exp(-\mathrm{i}\omega t)]$, so that

$$\langle\hat{\sigma}_+\rangle=\bar{\rho}_{12}, \tag{4.26}$$

and

$$\langle\hat{\sigma}_1^2\rangle=\langle\hat{\sigma}_2^2\rangle=\tfrac{1}{4}, \tag{4.27}$$

with

$$\langle \hat{\sigma}_1 \rangle = \tfrac{1}{2}(\bar{\rho}_{12} + \bar{\rho}_{21}). \tag{4.28}$$

Using equations (4.14), (4.16) and (4.28) we find [50]

$$\langle \hat{\sigma}_1 \rangle^2 = \frac{\frac{1}{4}\Omega^2\Delta^2}{(\Delta^2 + \gamma^2 + \frac{1}{2}\Omega^2)^2}, \tag{4.29}$$

$$\langle (\Delta\sigma_1)^2 \rangle = \frac{1}{4} - \frac{1}{4}\frac{\Omega^2\Delta^2}{(\Delta^2 + \gamma^2 + \frac{1}{2}\Omega^2)^2}, \tag{4.30}$$

where the detuning $\Delta \equiv \omega_0 - \omega$.

Similarly for $\hat{\sigma}_2 \equiv (1/2\mathrm{i})[\hat{\Pi}^\dagger \exp(-\mathrm{i}\omega t) - \hat{\Pi} \exp(\mathrm{i}\omega t)]$,

$$\langle (\Delta\sigma_2)^2 \rangle = \frac{1}{4} - \frac{1}{4}\frac{\Omega^2\gamma^2}{(\Delta^2 + \gamma^2 + \frac{1}{2}\Omega^2)^2}. \tag{4.31}$$

The time-dependences can be calculated using the full time-dependent Bloch equation solutions of Torrey [52] and others (e.g. [51]). Dipole squeezing is produced if the detuning satisfies

$$\Delta^2 > \gamma^2 + \tfrac{1}{2}\Omega^2 \tag{4.32}$$

or

$$(\Delta/\gamma)^2 > (\Omega^2/2\gamma^2) + 1. \tag{4.33}$$

The dipole squeezing in equations (4.30) and (4.31) is not a minimum-uncertainty state squeezing.

The fluorescent field fluctuations from a laser-excited two-level atom are not always directly related in a simple fashion to dipole squeezing [53, 54]. It is possible to find situations in which a squeezed dipole generates a field that is *not* squeezed. Nevertheless, squeezing can be generated in the radiated field. Because the atomic dipole couples to *all* modes of the electromagnetic field, it is necessary to extend our definitions of field operators and commutators. The positive and negative frequency parts $\hat{\mathbf{E}}^+$ and $\hat{\mathbf{E}}^-$ of the total electric-field operator at position $\mathbf{R}$ can be decomposed into travelling-wave modes λ as in equation (4.5) and its conjugate for $\hat{\mathbf{E}}^-$. The field commutator is (e.g. [25])

$$\begin{aligned}[\hat{E}_\alpha^+, \hat{E}_\beta^-] &= \frac{\delta_{\alpha\beta}}{(2\pi)^3}\frac{8\pi}{3}\frac{\hbar}{2\varepsilon_0 c}\int k_\lambda^3 \, \mathrm{d}\mathbf{k}_\lambda \\ &\equiv C,\end{aligned} \tag{4.34}$$

where C is finite only if the mode sum (or integration) is cut off at some high frequency. In the far field, where the atomic source is situated a distance $|\mathbf{r} - \mathbf{R}| \gg \lambda$ from the detector, the field from a two-level atom is given by

$$\hat{\mathbf{E}}^\pm(\mathbf{r}, t) = \hat{\mathbf{E}}_\mathrm{f}^\pm(\mathbf{r}, t) + \hat{\mathbf{E}}_\mathrm{s}^\pm(\mathbf{r}, t), \tag{4.35}$$

where the source field $\hat{\mathbf{E}}_\mathrm{s}^\pm(\mathbf{r}, t)$ is given by equation (4.7) and $\hat{\mathbf{E}}_\mathrm{f}^\pm$ is the free, homogeneous field.

The radiated field quadrature operators (for the radiated field at a frequency close to ω) are

$$\hat{E}_1 = \tfrac{1}{2}[\hat{E}^+ \exp(i\omega t) + \hat{E}^- \exp(-i\omega t)], \tag{4.36}$$

$$\hat{E}_2 = \frac{1}{2i}[\hat{E}^+ \exp(i\omega t) - \hat{E}^- \exp(-i\omega t)] \tag{4.37}$$

so that

$$\hat{E} = 2\hat{E}_1 \cos\omega t + 2\hat{E}_2 \sin\omega t \tag{4.38}$$

and the quadrature commutator is

$$[\hat{E}_1, \hat{E}_2] = \tfrac{1}{2}iC, \tag{4.39}$$

with associated quadrature variances satisfying

$$\frac{\langle(\Delta E_1)^2\rangle}{C}\,\frac{\langle(\Delta E_2)^2\rangle}{C} \geqslant \frac{1}{16}. \tag{4.40}$$

It is also convenient to define normally ordered variances through

$$\frac{\langle :(\Delta\hat{E}_i)^2: \rangle}{C} = \frac{\langle(\Delta E_i)^2\rangle}{C} - \frac{1}{4}, \tag{4.41}$$

where $i = 1, 2$. For a coherent state, as well as for a vacuum state,

$$\frac{\langle(\Delta E_1)^2\rangle}{C} = \frac{1}{4} = \frac{\langle(\Delta E_2)^2\rangle}{C},$$

so that the squeezing criteria are

$$\langle(\Delta E_i)^2\rangle/C < \tfrac{1}{4} \tag{4.42}$$

or

$$\langle :(\Delta\hat{E}_i)^2: \rangle/C < 0, \tag{4.43}$$

for $i = 1$ or 2. Using equations (4.7) and (4.10) we have for the scattered source field

$$\langle \hat{E}_s^+ \exp(i\omega t)\rangle = \mu\tilde{\rho}_{21}. \tag{4.44}$$

The normally ordered variance of the source-field part of $\hat{E}_1$ is

$$\begin{aligned}\langle :(\Delta\hat{E}_1)^2: \rangle &= \tfrac{1}{4}[2\langle \hat{E}_s^- \hat{E}_s^+ \rangle - (\langle \hat{E}_s^+ \exp(i\omega t) + \hat{E}_s^- \exp(-i\omega t)\rangle)^2] \\ &= \tfrac{1}{4}[2|\mu|^2\langle \hat{\Pi}^\dagger\hat{\Pi}\rangle - (\mu\tilde{\rho}_{21} + \text{c.c.})^2].\end{aligned} \tag{4.45}$$

The first term is easily evaluated using

$$\hat{\Pi}^\dagger\hat{\Pi} = |2\rangle\langle 2| \tag{4.46}$$

so that (assuming for simplicity μ to be real) the normalized fluorescent field variance becomes

$$\langle :(\Delta\hat{E}_1)^2: \rangle/\mu^2 = [2\rho_{22} - (\tilde{\rho}_{12} + \tilde{\rho}_{21})^2] \tag{4.47}$$

or using equation (4.15) and (4.16)

$$\langle :(\Delta\hat{E}_1)^2: \rangle/\mu^2 = \frac{\frac{1}{2}\Omega^2(\gamma^2 + \frac{1}{2}\Omega^2 - \Delta^2)}{(\Delta^2 + \gamma^2 + \frac{1}{2}\Omega^2)^2}. \tag{4.48}$$

Similarly the normalized fluorescent $\hat{E}_2$ variance is given by

$$\langle :(\Delta\hat{E}_2)^2: \rangle/\mu^2 = \frac{\frac{1}{2}\Omega^2(\Delta^2 - \gamma^2 + \frac{1}{2}\Omega^2)}{(\Delta^2 + \gamma^2 + \frac{1}{2}\Omega^2)^2}. \tag{4.49}$$

Either $\hat{E}_1$ or $\hat{E}_2$ may be squeezed, depending on the detuning Δ. For example, $\langle :(\Delta\hat{E}_1)^2: \rangle/\mu^2$ is negative for $\Delta^2 > \gamma^2 + \frac{1}{2}\Omega^2$. Dalton [25] has studied the degree of squeezing produced in resonance fluorescence when further dissipative mechanisms (especially photoionization) exist.

Mandel [55] has discussed the connection between squeezed states and sub-Poissonian statistics and applied these considerations to the problem of resonance fluorescence. Barnett [53] and Wódkiewicz *et al.* [54] have examined the relationship between radiated field and dipole squeezing. In resonance fluorescence, we see from equations (4.5) and (4.6) that the positive-frequency part of the field is equal to a free contribution plus a term proportional to the dipole lowering operator. The normally ordered field variance is directly proportional to the normally ordered dipole variances. When an atom radiates into a single cavity field mode (for example in the Jaynes–Cummings system [e.g. 54], the relationship is much less straightforward, reflecting the non-Markovian evolution of atom and system variables.

When many two-level atoms are excited into phase-dependent Bloch states [56, 57], large amounts of squeezing of the collective atomic dipole operators are predicted [58, 59]. Bloch states may be prepared by coherent transient techniques such as photon echoes [51] and the squeezing is associated not with the quadratic, or two-photon coherent states $|\beta; \mu, \nu\rangle$ given by equation (3.6) but with SU(2) coherent states. Heidmann *et al.* [60] have also studied the effects of collective many-atom coupling to the radiation field on squeezing in fluorescence. Vaccaro and Pegg [61] have studied the squeezing of light when interacting with a coherently prepared collection of two-level atoms in an amplifier or attenuator. The coherent preparation can permit the amplification of squeezed light without destroying the squeezing. This is not possible for linear amplifiers possessing no initial phase coherence (e.g. [62]). A careful study of the properties of reservoirs with phase-dependent noise has been made by Stenholm and coworkers (e.g. [63] and references therein), who have called such systems 'rigged reservoirs'.

4.2. *The use of three-level atomic systems*

In two-level atomic sources of squeezed light, the nonlinearity which is responsible for squeezing is also associated with a significant population in the upper level. This will generate spontaneous emission which will produce excess quantum noise and spoil the squeezing. Three-level atomic lambda systems were suggested [64, 65] as sources of squeezed radiation that minimize upper-state population and spontaneous emission through the mechanism of population trapping (e.g. [66]). In a lambda system (figure 9) excited by two coherent laser fields, the ground-state coherences between states 0 and 2 destructively interfere and on two-photon or Raman resonance the excited-state population vanishes in steady state [67–70]. The atomic population is optically pumped into a stable dressed state [71, 72] consisting of an antisymmetric superposition of the ground states in which the atom is unable to fluoresce. Many such three-level lambda systems would form a nonlinear medium with large two-photon resonantly enhanced nonlinear optical polarizations suitable for the generation of squeezing but without the hindrance of atomic fluorescent noise. A large amount of squeezing has been predicted in the cavity field modes

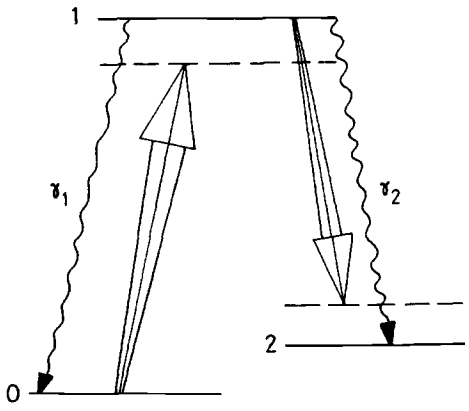

Figure 9. Stimulated and spontaneous transitions in a three-level atom. Laser excitation followed by fluorescence at rates γ_1 and γ_2 optically pump the atom into a coherent superposition of lower states 0 and 2.

involved in four-wave mixing and in optical bistability involving such three-level systems [73, 74].

Squeezing in three-level atom resonance fluorescence has been studied by de Oliveira *et al.* [75]. We saw earlier that the relaxation of the upper level may degrade squeezing by introducing extra phase-insensitive spontaneous emission noise. Population trapping [66] can drastically reduce, or even eliminate the upper-state population responsible for such noise, by optically pumping the population into a stable dressed superposition state. Population trapping is generated only at two-photon resonance. Nevertheless, the upper-state population reduction observed *near* to two-photon resonance may be of use if at this point the coherences ρ_{01} and ρ_{10} persist and provide a degree of phase-sensitive fluorescence. Unfortunately, for the three-level atomic system shown in figure 9 with no relaxation between the ground states $|0\rangle$ and $|2\rangle$, *no* steady-state squeezing is found to survive the optically pumped population trapping. Only if strong ground-state relaxation is allowed between $|0\rangle$ and $|2\rangle$ is squeezing recovered, and under these circumstances, the system behaves precisely as a two-level system.

The Hanle effect [76], involving fluorescence from a coherent superposition of atomic Zeeman sublevels, can also lead to squeezed radiation [77] which depends on the direction of emission.

4.3. *Prospects for generation of squeezed light using single cavity modes, co-operation and Rydberg atoms*

If an atom is optically excited in a high-Q cavity, the cavity mode radiation can be squeezed [78]. This squeezing can be modified by using several atoms in the cavity which collectively interact through their common radiation field. Butler and Drummond [79] have shown that a group of two-level atoms, initially in their ground states, induce squeezing in a coherent single-mode field. The multi-atom squeezing studied in [79], is produced only transiently, and can amount to a reduction of ~ 70 per cent in one of the field variances. Although it is extremely difficult to realize such single-mode field coupling to atomic transitions in normal optical experiments (although see [80]), this situation is more easily attainable in a microwave transition.

Unfortunately, normal microwave transitions have such weak coupling to radiation fields that quantum effects are entirely masked. A major innovation in the study of the effects of photon statistics in atom–field interactions has been the development of Rydberg-atom masers [81–86].

Rydberg atoms are highly excited atoms (for example, rubidium atoms have been excited to states with principal quantum numbers $n=65$ in recent atom–field interaction experiments) which have huge dipole moments, proportional to n^2 and couple extremely strongly to radiation fields [81, 82]. The resonance transition frequencies to nearby Rydberg levels lie in the sub-millimetre range so that transitions can be enhanced by high-Q cavities [83]. This combination of strong millimetre-wavelength transitions and high-Q cavities has lead to the development of Rydberg atom masers [84–86] which consist of a beam of (usually alkali) atoms, excited to high-lying Rydberg states by tunable lasers, which enter a tuned cavity resonant with a transition to a nearby level. The cavity is cooled by cryogenic techniques to minimize thermal background radiation (important in this long-wavelength region of the spectrum). Transitions can be monitored by state-selective ionization detection of the atoms as they leave the tuned cavity. Because the dipole moments of the transition are so large (orders of magnitude larger than the ammonia-maser transition at a comparable wavelength), the maser operating threshold can be so low that only a single Rydberg atom at a time in the cavity may be necessary for maser action. The Rydberg atom maser couples strongly to rather weak radiation fields so that its evolution critically depends on the statistics of the photons in the cavity and can sense the discreteness of the quantized single-mode maser field. The coherent Rabi oscillations as atom and field mode exchange energy resonantly are dephased by the residual vacuum quantum noise present even in a coherent state of the radiation, and the one photon–one atom interaction energy has been observed experimentally [87]. Under these circumstances it is clear that a suitably prepared atomic state which retains phase information could lead to squeezing in the Rydberg-atom maser field [88, 89].

Early theoretical studies of Rydberg maser squeezing were performed by Heidmann *et al.* [90–93] when many atoms collectively interact with the cavity field. Two different mechanisms for squeezing were described. The first involved the excitation of the atoms into a phase-sensitive collective atomic coherent state which radiates into the vacuum state of the cavity mode by super-radiant coupling (e.g. [81]). The second (often called 'triggered' superfluorescence) involves a wholly inverted atomic population radiating into a cavity mode prepared initially in a coherent state. In each case, large amounts of transient squeezing were predicted. Collective many-atom dipole squeezing has also been predicted through numerical studies of the co-operative evolution of up to 20 atoms driven coherently by an external field [94].

In the work of Heidmann *et al.* [90–93], the collective many-atom enhancement of the atom–field coupling was essential for the production of good squeezing. Nevertheless, squeezing may be generated even by a single atom interacting with a cavity field mode. Again, two types of initial phase-dependent preparation are possible: the atom may interact with a coherent-state field, or may be prepared in a coherent superposition state which spontaneously radiates. In the first, we are considering the famous Jaynes–Cummings model of quantum-optical resonance [95–97, 86, 87]. Were the initially unexcited atom to interact resonantly with a cavity field mode in a number state $|n\rangle$, the probability of the atom being excited

sinusoidally varies at the n-photon Rabi frequency [21]:

$$P_e(t)=\sin^2(n^{1/2}\lambda t), \tag{4.50}$$

where $2\lambda=d\mathscr{E}_0/\hbar$, d is the atomic transition dipole moment and $\mathscr{E}_0$ is the 'electric field per photon'. The inversion, defined as the difference between the excited- and ground-state probabilities evolves as

$$w_n(t)=-\cos(2n^{1/2}\lambda t). \tag{4.51}$$

In practice, the field mode will have a distribution of photon numbers $p(n)$. If the field is in a coherent state $|\alpha\rangle$, $p(n)$ is a Poisson distribution

$$p(n)=\frac{|\alpha|^{2n}}{n!}\exp(-|\alpha|^2) \tag{4.52}$$

with a mean $\langle\hat{n}\rangle=|\alpha|^2$ and a width $\Delta n=|\alpha|$. The inversion excited by an initially coherent field is then

$$w_\alpha(t)=-\sum_{n=0}^{\infty}\exp(-|\alpha|^2)\frac{|\alpha|^{2n}}{n!}\cos(2\lambda n^{1/2}t). \tag{4.53}$$

The Poisson spread in n dephases or 'collapses' the Rabi oscillations [96–105], which revive at later times owing to the discreteness of the summation [99–101]. The collapse time is λ^{-1} and the revival time is $2\pi|\alpha|/\lambda$, for an initially coherent field. More generally, in a field of arbitrary photon statistics, the collapse time is $t_c\sim\langle\hat{n}\rangle^{1/2}/\lambda\Delta n$, where Δn is the width of the photon number distribution. The Jaynes–Cummings collapses and revivals have recently been observed [87], using Rydberg-atom masers in ultra-high-Q cavities. Meystre and Zubairy [106] calculated the field variances for the cavity field quadrature operators $\hat{X}$ and $\hat{Y}$, and showed that a small amount of squeezing is produced in the Jaynes–Cummings model. The variances $\langle(\Delta X)^2\rangle$ and $\langle(\Delta Y)^2\rangle$ are given in terms of annihilation and creation operator expectation values by

$$\langle(\Delta X)^2\rangle=\tfrac{1}{4}(2\langle\hat{a}^\dagger\hat{a}\rangle+1+\langle\hat{a}^2\rangle+\langle\hat{a}^{\dagger 2}\rangle)-\tfrac{1}{4}\langle\hat{a}+\hat{a}^\dagger\rangle^2 \tag{4.54}$$

and

$$\langle(\Delta Y)^2\rangle=\tfrac{1}{4}(2\langle\hat{a}^\dagger\hat{a}\rangle+1-\langle\hat{a}^2\rangle-\langle\hat{a}^{\dagger 2}\rangle)+\tfrac{1}{4}\langle\hat{a}-\hat{a}^\dagger\rangle^2. \tag{4.55}$$

The field reduced density matrix for an atom initially in the excited state and the field initially in a coherent state $|\alpha\rangle$ is calculated by Meystre and Zubairy directly from the time-evolution operator $\hat{u}(t,0)$ given by

$$\hat{u}(t,0)=\exp(-i\hat{H}_I t/\hbar), \tag{4.56}$$

where $\hat{H}_I$ is the interaction Hamiltonian

$$\hat{H}_I=\hbar\lambda(\hat{\sigma}_+\hat{a}+\hat{\sigma}_-\hat{a}^\dagger). \tag{4.57}$$

The field reduced density operator at time t is

$$\hat{\rho}_f(t)=\mathrm{Tr}_{\mathrm{atom}}\left(\hat{u}(t,0)\begin{bmatrix}\hat{\rho}_f(0) & 0\\ 0 & 0\end{bmatrix}\hat{u}^\dagger(t,0)\right), \tag{4.58}$$

where $\hat{\rho}_f(0)$ is the initial field density operator. Evaluating the trace gives

$$\hat{\rho}_f(t) = \cos[\lambda t(\hat{a}\hat{a}^\dagger)^{1/2}]\hat{\rho}_f(0)\cos[\lambda t(\hat{a}\hat{a}^\dagger)^{1/2}] + \hat{a}^\dagger \frac{\sin[\lambda t(\hat{a}\hat{a}^\dagger)^{1/2}]}{(\hat{a}\hat{a}^\dagger)^{1/2}}\hat{\rho}_f(0)\frac{\sin[\lambda t(\hat{a}\hat{a}^\dagger)^{1/2}]}{(\hat{a}\hat{a}^\dagger)^{1/2}}\hat{a}. \quad (4.59)$$

The matrix element of $\hat{\rho}_f(t)$ in a number-state basis for an initially coherent field is from equation (4.59)

$$\begin{aligned}\rho_{nm}(t) &= \langle n|\hat{\rho}_f(t)|m\rangle \\ &= [\exp(-|\alpha|^2)\alpha^{n-1}(\alpha^*)^{m-1}/(n!m!)^{1/2}] \\ &\quad \times \{|\alpha|^2 \cos[\lambda t(n+1)^{1/2}]\cos[\lambda t(m+1)^{1/2}] \\ &\quad + (nm)^{1/2}\sin(\lambda t n^{1/2})\sin(\lambda t m^{1/2})\}. \end{aligned} \quad (4.60)$$

These density matrix elements enable us to calculate the cavity mode variances $\langle(\Delta X)^2\rangle$ and $\langle(\Delta Y)^2\rangle$ from equations (2.25)–(2.29). In figure 10 we plot the variance $\langle(\Delta X)^2\rangle$ for $\phi = 0$ (changing ϕ to $\pi/2$ turns $\langle(\Delta X)^2\rangle$ into $\langle(\Delta Y)^2\rangle$). Squeezing is produced at short times, and at later times when the Rabi oscillations have revived. The squeezing is small, but not insignificant for this most fundamental of quantum-optical problems. The detection of squeezing in Rydberg transitions is likely to be difficult [89].

Milburn [107] has examined the interesting question of how squeezed light interacts with atomic systems. We have seen above how the Rabi oscillations in the Jaynes–Cummings model collapse and revive in a manner that depends upon the photon statistics of the cavity field. Milburn uses the photon number distribution

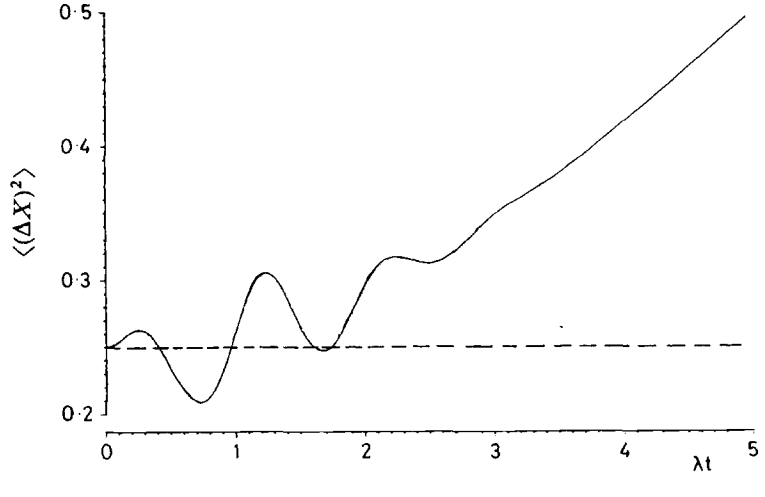

Figure 10. Variance $\langle(\Delta X)^2\rangle$ plotted against normalized time λt for the coherent-state Jaynes–Cummings model of a single atom interacting with a single field mode. The dashed line marks the vacuum noise variance. We have set the coherent field phase equal to zero and the mean photon number equal to ten.

$p(n)$ for squeezed single-mode cavity radiation (from equation (3.31)) to weight the Jaynes–Cummings inversion $w_n(t)$ given by equation (4.51)

$$\bar{w}(t) = -\sum_{n=0}^{\infty} p(n) \cos(2\lambda n^{1/2} t). \tag{4.61}$$

The photon number variance for $\theta = 0$ is given by (3.20) as

$$\langle (\Delta n)^2 \rangle = \tfrac{1}{2} \sinh^2(2s) + |\alpha|^2 [\cosh(2s) - \sinh(2s) \cos 2\phi], \tag{4.62}$$

where s is the squeezing amplitude, $|\alpha|$ and ϕ the amplitude and phase of the coherent part of the squeezed light. If $\phi = \pi/2$,

$$\langle (\Delta n)^2 \rangle = \langle \hat{n} \rangle \exp(2s) + \sinh^2 s[1 - \sinh(2s)], \tag{4.63}$$

whereas if $\phi = 0$

$$\langle (\Delta n)^2 \rangle = \langle \hat{n} \rangle \exp(-2s) + \sinh^2 s[1 + \sinh(2s)]. \tag{4.64}$$

If the coherent contribution to $\bar{n}$ is dominant,

$$\langle (\Delta n)^2 \rangle \approx \langle \hat{n} \rangle \exp(\pm 2s). \tag{4.65}$$

If the squeezing is in the same direction as the coherent amplitude, the photon number distribution is sub-Poissonian. If the squeezing is in the direction orthogonal to the coherent amplitude, the distribution is super-Poissonian (these are shown in figure 7). If $\alpha = 0$, the distribution is always broader than the Poissonian. Milburn [107] demonstrated that the collapse time for the inversion may be increased or decreased over that time expected for a coherent input, and that a squeezed *vacuum* produced a time-dependent inversion very similar to that of a thermal or Bose–Einstein field [103]. In the micromaser experiments of Walther *et al.* [87] it is expected that the cavity field will develop significant sub-Poissonian statistics [108, 109] which will affect their observed collapses and revivals along the lines suggested by Milburn [107].

5. Detection of squeezed light

5.1. *Direct detection*

Figure 11 shows schematically the simplest kind of photon-statistical experiment in which light of photon-number distribution P_n falls directly on a photodetector of quantum efficiency η. Suitable processing of the photocurrent provides the statistical distribution $P_m(T)$ of the number m of photocounts recorded during repeated time-intervals of duration T. The photocount distribution provides a record of the photon-number distribution distorted by the effects of the non-unit quantum efficiency η and the finite integration time T. The main requirement is the extraction of values for the photon-number mean and variance from measurements of the photocount mean and variance.

Consider first the effects of the non-unit quantum efficiency η of the photodetector. This can be modelled [110] by the arrangement shown in the dashed box in figure 11, where the inefficiency in detection is ascribed to the loss of light at a beam-splitter, which transmits only a fraction $\eta^{1/2}$ of the incident amplitude. The

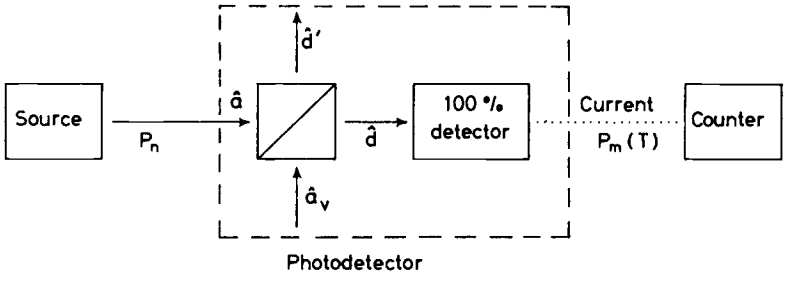

Figure 11. Schematic arrangement of direct-detection experiment. The beam-splitter and perfectly efficient detector in the dashed rectangle together model a photodetector of quantum efficiency η.

destruction operator at the detector is thus

$$\hat{d}=\eta^{1/2}\hat{a}+(1-\eta)^{1/2}\hat{a}_v, \tag{5.1}$$

where $\hat{a}_v$ represents an inevitable admixture of a vacuum field from the other input to the beam-splitter. The field represented by $\hat{d}$ is now assumed to be detected with 100 per cent efficiency. All normally ordered expectation values of the vacuum-field operators vanish, and it follows that

$$\langle\hat{d}^\dagger\hat{d}\rangle=\eta\langle\hat{a}^\dagger\hat{a}\rangle=\eta\langle\hat{n}\rangle \tag{5.2}$$

and

$$\langle\hat{d}^\dagger\hat{d}^\dagger\hat{d}\hat{d}\rangle=\eta^2\langle\hat{a}^\dagger\hat{a}^\dagger\hat{a}\hat{a}\rangle=\eta^2\langle\hat{n}(\hat{n}-1)\rangle. \tag{5.3}$$

The effects of the finite integration-time T depend upon its relation to the fluctuation time-scale of the detected light. For a single-mode input, the integration time is effectively short compared with the fluctuation period, and in this case no further distortion is introduced by the measurement process. The photocount mean and variance obtained from (5.2) and (5.3) are thus

$$\langle\hat{m}\rangle=\eta\langle\hat{n}\rangle \tag{5.4}$$

and

$$\langle(\Delta m)^2\rangle=\eta^2\langle(\Delta n)^2\rangle+\eta(1-\eta)\langle\hat{n}\rangle. \tag{5.5}$$

In these expressions, the photon numbers that appear should be interpreted as the photon flux, in units of quanta per unit time, multiplied by the integration time T.

The complete photocount distribution produced by direct detection of single-mode squeezed light has been derived by Walls *et al.* [111]. We consider here only the first two moments (5.4) and (5.5) of this distribution for the limiting case of squeezed light with a large coherent contribution, where use of the results (3.24) and (3.25) gives

$$\langle\hat{m}\rangle=\eta|\alpha|^2 \tag{5.6}$$

and

$$\langle(\Delta m)^2\rangle=\eta|\alpha|^2\{1+\eta[\exp(-2s)\cos^2(\phi-\tfrac{1}{2}\theta)+\exp(2s)\sin^2(\phi-\tfrac{1}{2}\theta)-1]\}. \tag{5.7}$$

The first unit term in the curly bracket produces the usual shot noise found in the detection of coherent light. The term in the square brackets is negative when the antibunching condition (3.27) is satisfied. The existence of antibunching in the light is thus manifested by a photocount variance smaller than the shot-noise value.

It is sometimes useful to characterize the detected noise in terms of a parameter Q_D defined by analogy with (2.44) as

$$Q_D = \frac{\langle (\Delta m)^2 \rangle - \langle \hat{m} \rangle}{\langle \hat{m} \rangle}. \tag{5.8}$$

It follows from (5.4) and (5.5) that in the limit of short integration times T,

$$Q_D = \eta Q. \tag{5.9}$$

Sub-Poissonian photon-number statistics, corresponding to negative Q, thus produce sub-Poissonian photocount statistics, indicated by a negative Q_D, however the magnitude of the non-classical effect is attenuated by the detector efficiency η.

The above outline of single-mode direct detection theory can be expanded to cover the more realistic situations in which the light falling on the detector is a continuous-mode excitation described by a spectral distribution of photon flux. The photodetection statistics then depend on the relative sizes of the spectral width and the detection bandwidth $1/T$. For the case of squeezed light produced by a degenerate parametric amplifier, with a coherent contribution to the flux much larger than the squeezing contribution, the photocount variance is again given by (5.7), when the detection bandwidth is much smaller than the spectral width [41]. The quantity $|\alpha|^2$ in (5.6) and (5.7) is here interpreted as the coherent flux multiplied by the integration time.

Direct-detection experiments are not specifically sensitive to squeezing in the input light, but only to the associated antibunching or sub-Poissonian statistics, both of which can also occur for non-squeezed light. We therefore proceed to consider phase-sensitive detection schemes that more clearly display any squeezing present in the input.

5.2. *Ordinary homodyne detection*

Figure 12 shows the schematic arrangement of a homodyne detector. The input signal mode with operator $\hat{a}$ is superposed on a local oscillator mode with operator $\hat{a}_L$ by a lossless symmetric beam-splitter, with amplitude reflection and transmission coefficients r and t. The output-mode destruction operators are given by

$$\begin{bmatrix} \hat{d}_1 \\ \hat{d}_2 \end{bmatrix} = \begin{bmatrix} r & t \\ t & r \end{bmatrix} \begin{bmatrix} \hat{a}_L \\ \hat{a} \end{bmatrix}, \tag{5.10}$$

where unitarity of the coupling matrix requires that

$$|r|^2 + |t|^2 = 1 \quad \text{and} \quad t^* r + r^* t = 0. \tag{5.11}$$

The quantum theory of homodyne detection was originated principally by Yuen and Shapiro [112, 113, 110]. Two basic varieties of detector are capable in principle of measuring quantum effects in the input signal noise. In *ordinary* homodyne detection, the beam-splitter coefficients satisfy

$$|r| \ll |t| \quad \text{(ordinary)} \tag{5.12}$$

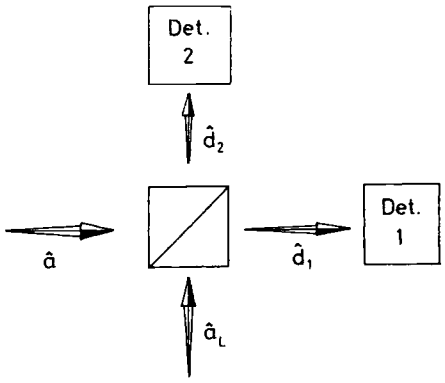

Figure 12. Schematic arrangement of a homodyne detector.

and only the output current from photodetector 1 is utilized. In *balanced* homodyne detection, the beam-splitter coefficients satisfy

$$|r| = |t| = 2^{-1/2} \quad \text{(balanced)} \tag{5.13}$$

and the output current for processing is formed from the difference of the two photodetector currents. The second condition in (5.11) is satisfied by

$$\arg r - \arg t = \tfrac{1}{2}\pi \tag{5.14}$$

for both kinds of homodyne detection.

Consider ordinary homodyne detection first, where the measured signal is determined by the operator

$$\hat{d}_1^\dagger \hat{d}_1 = |r|^2 \hat{a}_L^\dagger \hat{a}_L + t^* r \hat{a}^\dagger \hat{a}_L + r^* t \hat{a}_L^\dagger \hat{a} + |t|^2 \hat{a}^\dagger \hat{a}. \tag{5.15}$$

The input and local oscillator modes have the same frequency in homodyne detection, and the above operator is therefore time independent. With the local-oscillator light in a coherent state $|\alpha_L\rangle$, the operator expectation value is

$$\langle \hat{d}_1^\dagger \hat{d}_1 \rangle = |r|^2 |\alpha_L|^2 + 2|r|\,|t|\,|\alpha_L| \langle \hat{E}(\chi) \rangle + |t|^2 \langle \hat{a}^\dagger \hat{a} \rangle, \tag{5.16}$$

where

$$\hat{E}(\chi) = \tfrac{1}{2}[\exp(\mathrm{i}\chi)\,\hat{a}^\dagger + \exp(-\mathrm{i}\chi)\,\hat{a}] \tag{5.17}$$

is the field operator defined in (2.68), which is henceforth assumed to be expressed in units of the cavity field strength $\mathscr{E}_c$, and

$$\chi = \arg r - \arg t + \phi_L = \tfrac{1}{2}\pi + \phi_L. \tag{5.18}$$

Ordinary homodyne detectors normally use a strong local oscillator that satisfies the condition

$$|r|\,|\alpha_L| \gg |t|\,|\alpha|, \tag{5.19}$$

where α is the input signal complex amplitude. The inequalities (5.12) and (5.19) taken together imply that almost all of the input light reaches the photodetector, but even the small fraction of local-oscillator light reaching the detector still dominates

the input contribution. The terms on the right-hand side of (5.16) are thus in order of sharply diminishing magnitude, and the final term can be neglected. With the photon number in output mode 1 denoted n_1, the expectation value (5.16) can therefore be written

$$\langle n_1 \rangle = |r|^2 |\alpha_L|^2 + 2|r||t||\alpha_L| \langle \hat{E}(\chi) \rangle. \tag{5.20}$$

The photon-number variance for output mode 1 is calculated straightforwardly with the use of the number operator (5.15). With the inequality (5.19) satisfied, the dominant terms in the variance, of second order in $|\alpha_L|$, give

$$\langle (\Delta n_1)^2 \rangle = |r|^2 |\alpha_L|^2 [|r|^2 + 4|t|^2 \langle (\Delta E(\chi))^2 \rangle]. \tag{5.21}$$

Analogous to the discussion that follows (3.25), the two terms in (5.21) can be interpreted [114] as arising from the projections on to the reflected local-oscillator amplitude $|r||\alpha_L|$ of the reflected local-oscillator uncertainty and the transmitted input signal uncertainty, respectively. The inequality (5.12) ensures that the local-oscillator uncertainty is largely suppressed by the beam-splitter coupling, and the noise in ordinary homodyne detection is mainly determined by the input signal fluctuations.

The photocount mean and variance for a detector of quantum efficiency η are related to the corresponding photon-number quantities by expressions similar to (5.4) and (5.5). The larger contribution to the mean photocount comes from the first term in (5.20), but this has a known and fixed magnitude for a given detector, and its contribution can be subtracted from the detected quantity. The mean photocount after subtraction is

$$\begin{aligned} \langle m_1 \rangle &= 2\eta |r||t||\alpha_L| \langle \hat{E}(\chi) \rangle \\ &= 2\eta |r||t||\alpha_L||\alpha| \cos(\chi - \phi). \end{aligned} \tag{5.22}$$

This is similar to the expression found in the classical theory of homodyne detection. The photocount variance obtained with the use of (5.20) and (5.21) has a dominant term,

$$\langle (\Delta m_1)^2 \rangle = \eta |r|^2 |\alpha_L|^2 \{1 + \eta |t|^2 [4 \langle (\Delta E(\chi))^2 \rangle - 1]\}. \tag{5.23}$$

The contribution to this expression appearing in the square brackets vanishes for a coherent input, and the remaining contribution, from the 1 in the curly bracket, is the shot noise that characterizes the Poissonian photocount statistics that occur in this case. If the input field is squeezed, with

$$\langle (\Delta E(\chi))^2 \rangle < \tfrac{1}{4} \tag{5.24}$$

for some values of the angle χ, analogous to (2.72), then the photocount variance (5.23) is smaller than the shot-noise contribution alone. Thus squeezing in the input field operator $\hat{E}(\chi)$ is revealed in homodyne detection by sub-Poissonian photocount statistics [55]. The departure from the Poisson shot-noise variance shows a characteristic dependence on the local-oscillator phase, related to χ by (5.18).

The field variance for a squeezed-state input is easily shown with the aid of (3.7), (3.8) and (5.17) to have the form

$$\langle (\Delta E(\chi))^2 \rangle = \tfrac{1}{4} [\exp(-2s) \cos^2(\chi - \tfrac{1}{2}\theta) + \exp(2s) \sin^2(\chi - \tfrac{1}{2}\theta)]. \tag{5.25}$$

The squeezing condition (5.24) is satisfied for phase angles such that

$$\cos(2\chi-\theta)>\tanh s. \tag{5.26}$$

Substitution of (5.25) into (5.23) gives an expression for the photocount variance in homodyne detection that is very similar to the corresponding expression (5.7) for direct detection of squeezed light with a large coherent component. The connection occurs because the effect of the beam-splitter in homodyne detection is to transform an input ideal squeezed state according to

$$|\alpha,\zeta\rangle\rightarrow|r\alpha_{\mathrm{L}}+t\alpha,t\zeta\rangle. \tag{5.27}$$

The transformed state is another ideal squeezed state, which now has a large coherent component $r\alpha_{\mathrm{L}}$, and the theory of § 5.1 is valid for the subsequent direct detection of the transformed state. Note however that the mean and the variance in homodyne detection, given by (5.22), (5.23) and (5.25), have phase dependences that can be studied by variation of the local-oscillator phase angle in accordance with (5.18). By contrast, the mean and the variance in direct detection, given by (5.4) and (5.7), are fixed by the parameters of the input squeezed light.

The mean (5.22) and the variance (5.25) of the field operator (5.17) that determines the characteristics of a homodyne measurement can be represented on the ideal-squeezed-state diagram in figure 4 by the projection of the coherent amplitude and the uncertainty ellipse on to an axis inclined at an angle χ to the X-axis. This 'homodyne' axis, shown dashed, rotates through 2π as the phase ϕ_{L} of the local oscillator is varied over the same range.

The mean homodyne field $\langle\hat{E}(\chi)\rangle$ is zero for a squeezed vacuum-state input, and the dependence of the field variance (5.25) on the detection phase angle χ can be studied in isolation. Figure 13 shows the square root of the field variance represented by a noise band that pulsates as the phase angle is varied with respect to $\frac{1}{2}\theta$. The variance has extremal values

$$\left.\begin{aligned}\langle[\Delta E(\tfrac{1}{2}\theta)]^2\rangle&=\tfrac{1}{4}\exp(-2s),\\ \langle[\Delta E(\tfrac{1}{2}\theta+\tfrac{1}{2}\pi)]^2\rangle&=\tfrac{1}{4}\exp(2s),\end{aligned}\right\} \tag{5.28}$$

that minimize the uncertainty product (2.70) for a specific pair of phase angles 90° apart.

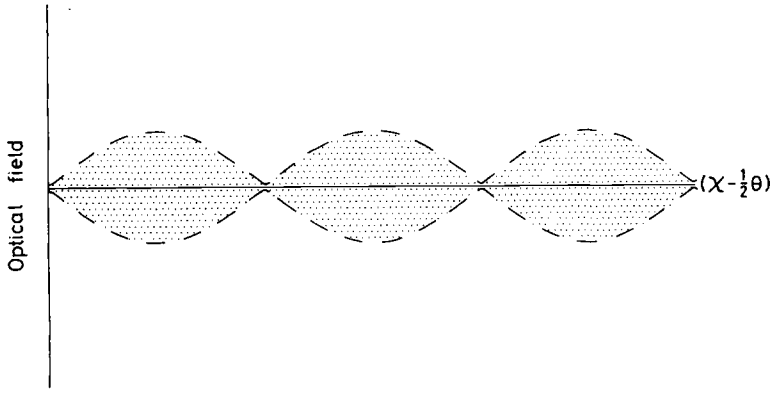

Figure 13. Phase dependence of the square root of the field variance for the squeezed vacuum state with $s=1{\cdot}5$.

For a squeezed-state input in which $|\alpha|$ is non-zero, the noise band shown in figure 13 now dresses the cosine wave associated with the mean homodyne field in equation (5.22). The phase angles ϕ and $\frac{1}{2}\theta$ of the mean and the variance, respectively, can be chosen independently. The special case

$$\tfrac{1}{2}\theta = \phi \tag{5.29}$$

has some advantages for applications of squeezed states since minimum noise coincides with the angles of maximum field amplitude, where the information content of a wave is often concentrated. Figures 1 and 2 show the phase dependences of the detected mean field and variance in this case for a coherent state and a squeezed state. By way of contrast, figure 14 shows a similar curve for mean and variance phase angles that differ by $\frac{1}{2}\pi$. This represents an input state whose phase angle is detected with a higher resolution than that of a coherent state, at the expense of a poorer definition of the wave amplitude.

The results of the single-mode theory outlined in the present subsection are unchanged for homodyne detection of continuum-mode ideal squeezed light whose spectral width is much larger than the detection bandwidth [41].

5.3. *Balanced homodyne detection*

We now consider the alternative scheme of balanced homodyne detection, where the difference of the two photodetector readings is taken for the schematic arrangement of figure 12. The output mode operators are determined by (5.10), with the beam-splitter parameters given by (5.13) and (5.14). The measured signal is determined by the operator

$$\hat{d}_1^\dagger \hat{d}_1 - \hat{d}_2^\dagger \hat{d}_2 = \mathrm{i}(\hat{a}^\dagger \hat{a}_\mathrm{L} - \hat{a}_\mathrm{L}^\dagger \hat{a}), \tag{5.30}$$

and the mean difference photon number is

$$\langle n_{12} \rangle = \langle \hat{d}_1^\dagger \hat{d}_1 - \hat{d}_2^\dagger \hat{d}_2 \rangle = 2|\alpha_\mathrm{L}| \langle \hat{E}(\chi) \rangle, \tag{5.31}$$

where the definitions (5.17) and (5.18) have been used again. It is seen by comparing (5.31) with (5.16) or (5.20) that the balancing of the two detectors has removed the contributions that are made by the local oscillator and the input signal alone in

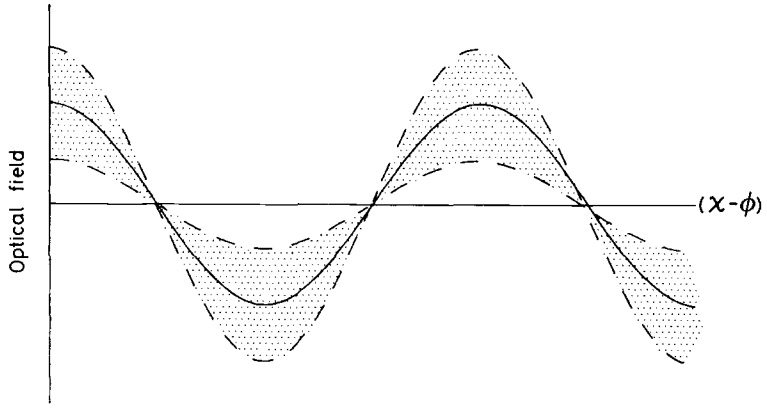

Figure 14. Phase dependence of the mean field and its uncertainty for squeezed light with a mean photon number $|\alpha|^2 = 4$, $s = 1{\cdot}5$ and phase angle $\phi = \theta/2 + \pi/2$.

ordinary homodyne detection, and only the important cross-term now survives. The variance of the operator (5.30) is easily shown to be

$$\langle(\Delta n_{12})^2\rangle = 4|\alpha_L|^2\langle[\Delta E(\chi)]^2\rangle, \tag{5.32}$$

where the local oscillator is still assumed to be much stronger than the input signal, with

$$|\alpha_L|^2 \gg |\alpha|^2; \tag{5.33}$$

note, however, that this requirement on local-oscillator strength is less stringent than that for ordinary homodyne detection, expressed by the inequalities (5.12) and (5.19). It is seen by comparing (5.32) with (5.21) that the balancing has eliminated the local-oscillator contribution to the noise completely, and this constitutes a major advantage of the difference-detection scheme [110, 115, 116]. The corresponding expressions for the photocount mean and variance are

$$\langle m_{12}\rangle = 2\eta|\alpha_L|\langle\hat{E}(\chi)\rangle \tag{5.34}$$

and

$$\langle(\Delta m_{12})^2\rangle = \eta|\alpha_L|^2\{1+\eta[4\langle[\Delta E(\chi)]^2\rangle - 1]\}. \tag{5.35}$$

The remarks made above in connection with the corresponding expression (5.23) for ordinary homodyne detection continue to apply for balanced homodyne detection with only minor changes.

The balanced homodyne detector of figure 12 is essentially a four-port device, with two inputs and two outputs, and it measures a single quadrature component of the input field. Figure 15 shows a more elaborate eight-port homodyne detector [117, 118], in which the differences of the photodetector readings 1, 2 and 3, 4 are taken. It is not difficult to show that the mean difference photocounts are

$$\left.\begin{aligned}\langle m_{12}\rangle &= \eta|\alpha_L|\langle\hat{E}(\chi+\tfrac{1}{2}\pi)\rangle,\\ \langle m_{34}\rangle &= \eta|\alpha_L|\langle\hat{E}(\chi)\rangle,\end{aligned}\right\} \tag{5.36}$$

where all four beam-splitters have the properties (5.13) and (5.14), and the local-oscillator light is a coherent state $|\alpha_L\rangle$. The eight-port detector thus measures two quadrature components of the input field, with phases determined by the angle χ defined in (5.18).

The difference photocount variances are also readily calculated, with the results

$$\left.\begin{aligned}\langle(\Delta m_{12})^2\rangle &= \tfrac{1}{4}\eta|\alpha_L|^2\{2+\eta[4\langle[\Delta E(\chi+\tfrac{1}{2}\pi)]^2\rangle - 1]\},\\ \langle(\Delta m_{34})^2\rangle &= \tfrac{1}{4}\eta|\alpha_L|^2\{2+\eta[4\langle[\Delta E(\chi)]^2\rangle - 1]\}.\end{aligned}\right\} \tag{5.37}$$

It is seen by comparison with the four-port result (5.35) that, because the 1 in the curly bracket has been replaced by 2 in (5.37), the photocount variances are no longer determined solely by the input-field variances, even in the limit of perfect detection ($\eta = 1$). The additional contributions to the photocount fluctuations in the eight-port device can be traced to vacuum fluctuations in the two unused input ports, shown dashed in figure 15. The additional uncertainty also provides an illustration of general requirements that apply to the simultaneous measurement of any pair of conjugate observables [119]. The outputs from an eight-port detector could in principle be used to provide an XY display of the uncertainty ellipse of an input ideal squeezed state, similar to that shown in figures 5 or 6, but with the additional spread

associated with the detection process itself. Practical displays of this kind have been produced for input coherent light [117]. Walker has shown [118] that the additional noise produced by a general homodyne detector, with arbitrary numbers of ports, can always be described by the convolution of a 'detector squeezed state' with the state of the input field. The four-port and the eight-port detectors with identical symmetrical beam-splitters treated above correspond to limiting cases in which the detector squeezed state is respectively a line state ($s\rightarrow\infty$) and a coherent state ($s\rightarrow 0$) [114, 120].

5.4. *Heterodyne detection*

Heterodyne detection is ideally suited to measurements on the two-mode squeezed states described in § 3.4, where the squeezing is carried jointly by modes of frequency ω_+ and ω_-. The experimental arrangement is the same as that shown in figure 12, but the local oscillator how has a frequency ω_L midway between ω_+ and ω_-. The detected photocurrent component that oscillates at the intermediate frequency

$$\omega_I=\omega_+-\omega_L=\omega_L-\omega_- \tag{5.38}$$

thus depends on the excitation in both modes, and in particular on the cross-correlations (3.43) that give rise to the squeezing effect.

The quantity measured in a heterodyne detector is a two-component generalization of the field (2.68) of the form

$$\hat{E}(\chi)=\tfrac{1}{2}\mathscr{E}_{c+}[\exp(i\chi)\,\hat{a}_+^\dagger+\exp(-i\chi)\,\hat{a}_+]+\tfrac{1}{2}\mathscr{E}_{c-}[\exp(i\chi)\,\hat{a}_-^\dagger+\exp(-i\chi)\,\hat{a}_-], \tag{5.39}$$

where the prefactors, given by generalizations of equations (1.1) and (2.6), include the square roots of the mode frequencies. The ionization rates in the photodetectors are determined by this field operator, with the $\omega_\pm^{1/2}$ factors in place [37]. Further, frequency dependence in the detection process results from variations in the ionization density of states, which may be significantly different at the frequencies ω_+ and ω_-. These effects tend to diminish the influence of the input squeezing on the measured photocurrents.

In many cases, however, the mode frequencies are sufficiently close together that differences between their square roots and their photoionization rates can be neglected. The prefactors in equation (5.39) can then be set equal to a common factor $\mathscr{E}_c$ evaluated at the local-oscillator frequency ω_L. The detected means and variances are thus expressed in terms of renormalized field operators analogous to $\hat{E}(\chi)$ in (5.17). The operator $\hat{X}$ in equation (3.44) is an example of such operators for the case $\chi=0$. As has been shown in (3.46), the two-mode variance of the operator $\hat{X}$ is identical with its single-mode counterpart given in (3.10), and this equivalence carries over to the detected quantities. Thus heterodyne detection of two-mode squeezed light is characterized by a photocount noise that is reduced below the value for coherent input light to the same extent as in homodyne detection of single-mode squeezed light. The same equivalence remains valid when the spectral distribution of multimode non-degenerate squeezed light is taken into account [41].

6. Generation of the squeezed states of light

6.1. *Introduction*

A nonlinear optical interaction will modify the noise properties of light by preferentially coupling to large-amplitude fluctuations. For example, an interaction

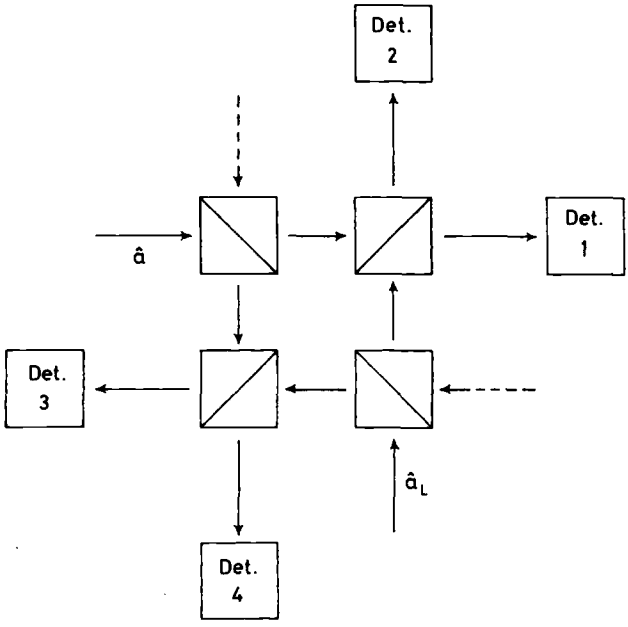

Figure 15. Schematic arrangement of an eight-port balanced homodyne detector.

which depends quadratically on the instantaneous field intensity, such as two-photon absorption or frequency doubling, is much more effective at the peak of an intensity fluctuation than in a low-intensity trough. This quadratic interaction will therefore preferentially absorb from the peaks and reduce the intensity (or amplitude) fluctuations. Conversely, a saturated absorber will act as a filter, allowing through large fluctuation peaks but suppressing troughs and increasing the amplitude fluctuations. This amplification or suppression of fluctuations is well known for classical stochastic noise and forms the basis of at least one successful type of laser mode-locking and short-pulse generation. The generation of squeezed light entails the extension of this nonlinear noise suppression to cover quantum fluctuations of light amplitude or phases. Phase sensitivity may be achieved by exploiting parametric resonance to amplify or attenuate optical fields through an interaction which depends on the phase of the driving field relative to the evolution of the parametrically excited material polarization. A simple example of parametric phase-sensitive resonance is that of the motion of a child on a swing, the amplitude of which may be increased by standing at the midpoint and sitting at the endpoints of the swing. Reversing the phase of the sitting and standing attenuates the swing motion. Noise fluctuations may be affected similarly, with phase-dependent noise amplification or suppression.

The simplest quadratic nonlinear optical interaction is described by the Hamiltonian (e.g. [3])

$$\hat{H} = \hbar[\chi^{(n)*}(\mathscr{E})\hat{a}^2 + \chi^{(n)}(\mathscr{E})\hat{a}^{\dagger 2}], \tag{6.1}$$

where the annihilation and creation operators $\hat{a}$, $\hat{a}^\dagger$ describe the quantized light-field mode of interest, and $\chi^{(n)}(\mathscr{E})$ is the effective nonlinear susceptibility, which depends

on the (classical) pump or driving field $\mathscr{E}$. A degenerate parametric amplifier is described by

$$\chi^{(2)}(\mathscr{E}) = \mathscr{E}\chi^{(2)} \tag{6.2}$$

and depends linearly on the classical pump field $\mathscr{E}$ and on the second-order nonlinear susceptibility $\chi^{(2)}$. Degenerate four-wave mixing (DFWM) is described by

$$\chi^{(3)}(\mathscr{E}) = \mathscr{E}^2\chi^{(3)} \tag{6.3}$$

and depends quadratically on pump field $\mathscr{E}$ and on the third-order susceptibility $\chi^{(3)}$. In both cases the quadratic dependence on the quantized field in equation (6.1) may lead to squeezed output. If the initial field state is the vacuum state, then the vacuum noise may be suppressed in a phase-sensitive manner. After a time t has elapsed, the interaction transforms the field state to the squeezed vacuum state

$$\begin{aligned} |t\rangle = |0, \zeta\rangle &= \exp(-i\hat{H}t/\hbar)\,|0\rangle \\ &= \exp(\tfrac{1}{2}\zeta^*\hat{a}^2 - \tfrac{1}{2}\zeta\hat{a}^{\dagger 2})\,|0\rangle, \end{aligned} \tag{6.4}$$

where the squeeze parameter is

$$\zeta = 2i\chi^{(n)}t. \tag{6.5}$$

The simplest quadratic interaction in nonlinear optics will therefore lead to an *ideal* squeezed vacuum state. Of course, the fluctuations, in the pump field (either classical stochastic or quantum) and dissipative losses will act to spoil the squeezing and will need to be minimized in a practical realization. In this section we will review progress towards the generation of strongly squeezed light in the laboratory.

6.2. *Quantum effects and field attenuation*

A first difficulty in the study of quantum non-classical fields is the non-trivial influence on the photon statistics of a linear attenuator. A quantum state of the field generated, for example in a nonlinear cavity, couples to the outside world through partially transmitting mirrors, beam-splitters and so on. If the intensity loss in traversing a linear loss element is η, the field is attenuated by a factor $\eta^{1/2}$. But the effect of η is not a mere scaling of the photon number [3] and was discussed in § 5.1. For example, if a field can be generated inside an optical cavity with no photon-number fluctuations, $\langle(\Delta n)^2\rangle = 0$, after traversing a linear loss element η, the photon-number variance outside is given by equation (5.5)

$$\langle(\Delta n)^2_{\text{out}}\rangle = (1-\eta)\langle\hat{n}_{\text{out}}\rangle, \tag{6.6}$$

where $\langle\hat{n}_{\text{out}}\rangle$ is the attenuated photon number. Linear attenuation generates fluctuations in an initially non-fluctuating field [115, 116, 121] reminiscent of the fluctuation-dissipation theorem. Squeezed light is extraordinarily fragile and may be degraded even by a beam-splitter or a mirror (as shown in § 5.1). A partially transmitting mirror may admit nothing from the outside world, but unfortunately 'nothing' is rather noisy; the vacuum fluctuations exceed the squeezed fluctuations that we are interested in generating! For this reason, great care must be taken to design optical systems that retain field squeezing and which do not admit vacuum noise.

6.3. *Four-wave mixing*

Yuen and Shapiro [122] were the first to suggest that degenerate backward four-wave mixing could generate squeezed light, which could be detected by homodyne beating. A phase-conjugate material pumped by two counter-propagating intense waves can generate a phase-conjugate signal in a wave travelling against an incoming probe wave. If we describe the incoming mode in terms of annihilation and creation operators $\hat{a}, \hat{a}^\dagger$, then the phase-conjugate reflected mode is described by the annihilation operator

$$\hat{b} = \mu\hat{a} + \nu\hat{a}^\dagger \tag{6.7}$$

with $\mu^2 - \nu^2 = 1$. If the incident field is in a coherent state then the phase-conjugate wave will be in an ideal squeezed state [12]. A high nonlinearity $\chi^{(3)}$ is required for large squeezing and this suggests that resonantly enhanced four-wave mixing should be employed. Whenever resonance is important, excitation in the medium must be included dynamically by going beyond a simple susceptibility formula, and spontaneous emission into the field modes of interest needs to be considered as an additional noise source [123–125]. To avoid excessive spontaneous emission noise, but to exploit near-resonance are demands which cannot simultaneously be satisfied and a compromise detuning must be chosen at an appreciable number of atomic linewidths from resonance. In addition, if the four-wave mixing takes place in free space rather than in a cavity, then the spatial coherence of the radiated field is likely to be poor and will degrade the squeezing [60].

6.4. *Second-harmonic generation in crystals*

As we noted in § 6.1, second-harmonic generation is also a candidate to generate squeezed light. This mechanism is not likely to suffer from spontaneous-noise problems, can be employed in crystals with large nonlinear susceptibilities and can be phase-matched using well-understood methods. Kozierowski and Tanaś [126] showed that the output light both at the fundamental and at the second-harmonic frequency has sub-Poissonian photon statistics. Mandel [127] has shown that this is accompanied by a small amount of squeezing, given the practical limitations on the length of the frequency-doubling crystal. The interaction time can be increased by perhaps two orders of magnitude if the frequency doubling is effected in an optical cavity, resonant at both fundamental and second harmonic [128] but the maximum amount of squeezing produced was only one-half the vacuum noise. This maximum squeezing is possible only at the oscillation threshold [129] for the growth of the intracavity harmonic. Again cavity damping destroys the squeezing as extra cavity-mode vacuum fluctuations add noise to the optical output.

6.5. *Parametric amplifiers and other sources of squeezing*

The degenerate parametric amplifier was the earliest candidate suggested to produce squeezed light [6, 8]. It acts by a second-order susceptibility and generates down-converted light at one-half the strong-pump wave frequency. The strong quantum correlations between the two down-converted photons are responsible for the squeezing. We note from equations (6.1) and (6.2) that a degenerate parametric amplifier driven by a strong classical pump field will generate ideal squeezed light (actually a squeezed vacuum). Nevertheless any phase fluctuations in the pump field (either through quantum [130–133] or through classical [134] noise fluctuations) will mix the quadratures $\hat{X}$ and $\hat{Y}$ and degrade the squeezing. A full quantum theory of

parametric amplification has been developed [130–133] which includes a quantized pump and cavity losses for both pump and subharmonic waves. If the damping rate of the pump wave far exceeds that of the sub-harmonic, then the pump degrees of freedom may be adiabatically eliminated and quadrature variances for the sub-harmonic field calculated in terms of hypergeometric functions [130–131] using a positive P-representation and Fokker–Planck equations developed earlier [135]. The minimum variance for the squeezing predicted was again only one-half the vacuum noise, achieved at the threshold for parametric oscillation in the cavity. Provided the pump field is maintained well *below* the parametric oscillation threshold, the positive P-distribution calculated by Milburn and Walls [130] agreed with that for an ideal squeezed state. This limiting factor of two in the reduced variance, precisely as found in the intracavity harmonic generation, suggested a fundamental limitation to the squeezing achievable in a symmetric linear cavity.

Several other nonlinear optical interactions have been proposed as sources of squeezed light. An optically bistable cavity containing a nonlinear medium in a high-finesse cavity driven by an external pump field is predicted to lead to squeezed light [136–138]. An absorbing medium which simultaneously absorbs several photons is clearly related to harmonic generation and leads to squeezing in the pump light [139].

6.6. *Successful demonstration of squeezing*

The limited squeezing predicted by the most promising nonlinear optical techniques was obtained in symmetric cavities. Yurke [140] made the important observation that asymmetric cavities, especially those with a single output port do not suffer from such limitations and can generate large amounts of squeezing. Essentially the limitations arise because of vacuum fluctuations which enter the cavity through the two partially transmitting mirrors. These may be eliminated in a ring cavity or a single-output linear cavity with the second mirror being perfectly reflecting. If inside the cavity the field is *perfectly* squeezed, then the variance in the transmitted output light may be calculated in terms of the mirror reflectivities. For a linear cavity formed by mirrors with intensity reflectivities R_1 and R_2, and transmissivities $T_1 = 1 - R_1$ and $T_2 = 1 - R_2$, then the variance outside a cavity with perfectly squeezed light inside is [140, 3]

$$\langle (\Delta X)^2 \rangle = \frac{1}{4} - \frac{T_1}{4(T_1 + T_2)}. \tag{6.8}$$

This simple relationship between the variances inside and outside the optical cavity was confirmed by detailed multimode calculations, provided the central frequency component in the squeezing spectrum is observed [39, 141–143]. It suggests that practical squeezing devices may be constructed using the techniques discussed earlier in this section provided asymmetric cavities are employed.

(i) *Four-wave mixing in sodium atoms*

The first pioneering observation of squeezed light was made by Slusher and coworkers at AT&T Bell Laboratories in 1985 [15]. They employed non-degenerate four-wave mixing in an atomic beam of sodium atoms pumped by dye-laser light (figure 16) and traversing an asymmetric cavity with essentially only a single output port, and found the quadrature noise could be reduced by 7–10 per cent below the vacuum or 'shot-noise' limit. The squeezing-cavity mirror reflectivities were 0·995

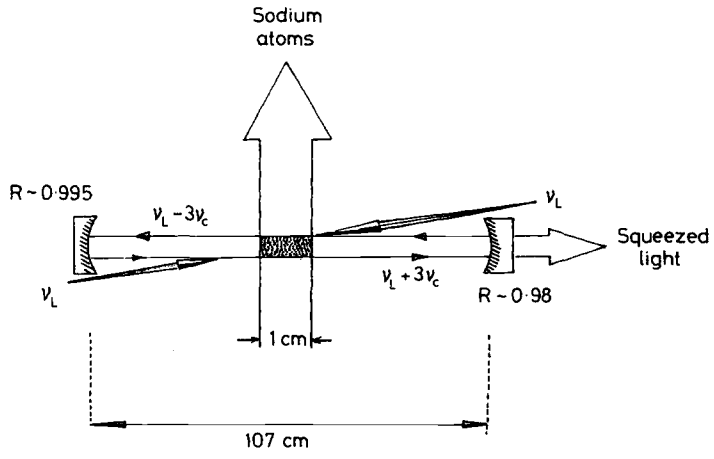

Figure 16. Schematic arrangement of four-wave mixing experiment in a sodium atomic beam to generate squeezed light [15]. The two counterpropagating pump waves of frequency ν_L excite sodium atoms traversing an asymmetric squeezing cavity with mirror reflectivities $R \sim 0{\cdot}995$ and 0·98 for the phase-conjugate pairs at $\nu_L \pm 3\nu_c$ where ν_c is the cavity mode spacing.

and 0·98. The nonlinear optical interaction took place in a beam of sodium atoms having a beam diameter of 1 cm generated by a Mach 2 supersonic nozzle, collimated to reduce the Doppler width seen by the near-tangential pump beams to 100 MHz, and with an atomic density of 10^{11} and 10^{12} atoms cm^{-3}. The pump waves were chosen to have a frequency ν_L detuned $\Delta = 1{\cdot}5$ GHz on the high-frequency side of the D_2 absorption line at about 589 nm, which is close enough to resonance to enhance the nonlinear mixing (proportional to Δ^{-3}, where Δ is the detuning) but far enough away to reduce the spontaneous-emission noise (proportional to Δ^{-2}). The saturation intensity at this detuning is about 1 kW cm^{-2} and the dye-laser pump intensity is 1/10 of this saturation value, over an area of 0·01 cm^2 of atomic beam.

The two pump waves generate a refractive-index wave at $2\nu_L$ which interacts with pairs of field modes at frequencies symmetrically displaced on either side of ν_L. The interaction strongly correlates the light in these mode pairs, at frequencies

$$\nu_{1,2} = \nu_L \pm n\nu_c, \tag{6.9}$$

where $n = 1, 2, \ldots$ and ν_c is the cavity-mode frequency spacing. This correlation leads to two-mode squeezing of the kind discussed in § 3.4 and detected by, for example, the heterodyne method discussed in § 5.4. All pairs of modes will exhibit two-mode squeezing, and Slusher *et al.* pick out pairs at cavity resonance frequencies $\nu_{1,2} = \nu_L \pm 3\nu_c$ to study because $3\nu_c \sim 0{\cdot}42$ GHz is sufficiently far from resonance for the spontaneous noise to be small. At these frequencies, the vacuum noise derives from the half-photon per mode zero-point fluctuations as always, whereas the spontaneous noise derives from less than (1/12) of a photon per mode.

The frequency and phase of the pump beams must be carefully stabilized to preserve the squeezing, so the pump laser is frequency stabilized to better than 0·1 MHz, and the pump intensity built up in a secondary confocal cavity not quite collinear with the squeezing cavity. No input is provided to the squeezing cavity, so

the squeezing is of the two-mode vacuum kind. Part of the pump beam is also used as the local oscillator in a homodyne detector and the noise levels recorded as the local oscillator phase varies as described earlier. The first results indicate squeezing of 7–10 per cent below the vacuum noise; improvements to the system bring the squeezing up to 20 per cent.

(ii) *Four-wave mixing in an optical fibre*

The second experiment which reported the observation of squeezed light also involved non-degenerate four-wave mixing, but in 100 m of optical fibre [16] excited by krypton-ion laser light. The interaction length l permitted by a fibre can be much longer than in a conventional nonlinear optical crystal, and ring interferometers containing optical directional couplers can permit single-output optical cavities [144, 145]. This system was expected to be free of noise but two noise sources in fact operate. The first is stimulated Brillouin scattering, which can be reduced or eliminated by using Faraday rotation isolators. The second is a new and more serious noise source termed GAWBS (guided acoustic-wave Brillouin scattering) which randomly modulates the pump wave and adds noise to nearby frequency bands which would otherwise be squeezed. The noise from GAWBS was only reduced by cooling the entire fibre interferometer in superfluid helium cooled below 4·2 K.

The nonlinear optical interaction used in the fibre was forward four-wave mixing based on coherent anti-Stokes Raman scattering (CARS) where two pump-photons generate sideband photons at frequencies ω_I and ω_S

$$\omega_S+\omega_I=2\omega_P \tag{6.10}$$

so that the sideband separation is $\omega_S-\omega_P=\omega_P-\omega_I=\Omega$. The two modes at ω_S, ω_I become strongly correlated through the nonlinear interaction, and this leads to two-mode squeezing. The two modes involved in the squeezing again are symmetrically displaced from the pump frequency. We concentrate on those fibre interferometer modes closest on either side of the pump mode, described by annihilation and creation operators $\hat{a}_\pm$ and $\hat{a}_\pm^\dagger$, and with a damping rate Γ_c determined by the cavity. The $(\pm)$ modes oscillate at frequencies $\pm m\Omega_c$, where Ω_c is the cavity-mode separation $\Omega_c=2\pi c/nl$ (n is the refractive index). The fibre four-wave mixing is described by the Hamiltonian [145]

$$\begin{aligned}\hat{H}=\hbar[(\Omega_p+m\Omega_c)\hat{a}_+^\dagger\hat{a}_+ &+(\Omega_p-m\Omega_c)\hat{a}_-^\dagger\hat{a}_-]+\hbar\chi^{(3)}[4|\tilde{E}_p^c|^2(\hat{a}_+^\dagger\hat{a}_+ +\hat{a}_-^\dagger\hat{a}_-)\\ &+2(\tilde{E}_p^c)^2\hat{a}_+^\dagger\hat{a}_-^\dagger+2(\tilde{E}_p^c)^{*2}\hat{a}_+\hat{a}_-]+\hat{a}_+\hat{\Gamma}_c^\dagger+\hat{a}_-\hat{\Gamma}_c^\dagger+\hat{a}_+^\dagger\hat{\Gamma}_c+\hat{a}_-^\dagger\hat{\Gamma}_c,\end{aligned} \tag{6.11}$$

where the dissipative heat-bath operators representing the field mode damping in the cavity are given by $\hat{\Gamma}_c$ and the nonlinear susceptibility is $\chi^{(3)}$. The dimensionless pump electric field is denoted by $\tilde{E}_p^c$ which is given in terms of the electric field per photon $\mathscr{E}_0$ and the real optical field E_p^c by

$$E_p^c=\mathscr{E}_0'\tilde{E}_p^c \tag{6.12}$$

(where $\mathscr{E}_0'=\mathscr{E}_0/n$, and n is the refractive index). Apart from the cavity damping, the two-mode *coupling* in the interaction equation (6.11) is entirely equivalent to the two-mode squeezing transformation given by equation (3.37).

The squeeze parameter $s=|\zeta|$ for this interaction is given by

$$s=\frac{12\pi\omega}{nc}f\chi^{(3)}|E_p^c|^2 l\equiv\frac{4\pi\chi^{(3)}\bar{I}^c}{\Omega_c}, \tag{6.13}$$

where f is a mode overlap factor in the fibre [145] approximately equal to unity and $\bar{I}^c$ is the dimensionless pump intensity. For the fused-silica fibre employed at the krypton-ion pump laser wavelength 647 nm, the nonlinear susceptibility $\chi^{(3)}\sim 5\times 10^{-15}\,\mathrm{cm^3\,erg^{-1}}$. Shelby *et al.* [145] calculate the squeezing expected from equation (6.11) by developing c-number Langevin equations for the mode amplitudes and evaluating the variances for the linear combination of waves which exhibit squeezing,

$$\hat{c}=\tfrac{1}{2}(\hat{a}_+ +\hat{a}_-), \tag{6.14}$$

$$\hat{d}=\tfrac{1}{2}(\hat{a}_+ -\hat{a}_-). \tag{6.15}$$

They also project these modes into pairs of free-space modes according to the Collett–Walls–Gardiner technique [38, 39] to calculate the properties of the output waves.

When this fibre four-wave mixing technique was employed, Shelby *et al.* [16] were able to generate squeezed light with a noise reduction of $(12{\cdot}5\pm 0{\cdot}5)$ per cent below the vacuum level. They used a fibre interferometer of length 114 m immersed in superfluid helium to reduce the GAWBS noise. Unfortunately at such low temperatures the stimulated Brillouin scattering threshold intensity is very low, so the pump power is segmented amongst 25 frequency elements with a phase modulator. The squeezing thus generated is broadband squeezing, and is below the vacuum noise over a narrow frequency range restricted by the GAWBS noise. This squeezing is detected by heterodyne beating.

(iii) *Parametric oscillation in lithium niobate*

The final experiment reporting the generation of squeezed light, which we will discuss, uses parametric amplification in a resonant asymmetric cavity [17] to generate minimum-uncertainty-state squeezing with a 63 per cent reduction in noise below the vacuum limit. The parametric oscillator used consisted of a lithium niobate crystal in a doubly resonant cavity with mirrors which almost completely reflect both pump and subharmonic light (figure 17). The mirrors are selected asymmetrically so that effectively only one output port for the subharmonic light exists. The squeezed light is detected by a balanced homodyne technique.

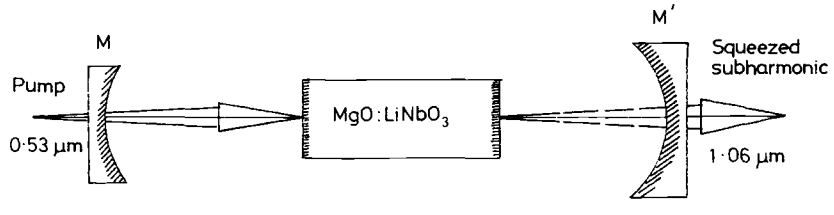

Figure 17. Schematic arrangement of parametric amplification in lithium niobate in an asymmetric cavity to generate squeezed light [17]. The pump light at 0·53 μm generates subharmonic light at 1·06 μm which is squeezed.

The cavity consists of two mirrors, M and M′ separated by 100 mm whose length is servocontrolled with r.f. sideband locking to preserve the sense of quadratures. The mirror M is the input mirror for the pump light at 0·53 μm and is 3·5 per cent transmitting for 0·53 μm pump light and 0·06 per cent for the subharmonic light at 1·06 μm. The mirror M′ is the output mirror for the subharmonic and is either 4·3 per cent or 7·3 per cent transmitting at 1·06 μm but with a very low transmission for the pump light at 0·53 μm. The parametric-oscillator crystal is made of $MgO:LiNbO_3$ (which generates a large $\chi^{(2)}$), is $25\times9\times9$ mm, heated to the phase-matching temperature of 98°C and is coated to minimize pump and subharmonic light losses. The pump radiation at 0·53 μm is derived by frequency-doubling light from a ring Nd:YAG laser using a BANANA doubler ($Ba_2NaNb_5O_{15}$) inside the laser cavity.

The pump amplitude fluctuations are deduced from balanced homodyne measurements to be at the shot-noise or vacuum level to within ±2 per cent at frequencies above 1 MHz. The detector is a balanced homodyne system [115] whose local oscillator is the fundamental of the Nd:YAG laser. The detector measures the fluctuations on the operator (equation (2.68))

$$\hat{E}(\chi)=\tfrac{1}{2}\mathscr{E}_c[\exp(i\chi)\,\hat{a}^\dagger+\exp(-i\chi)\,\hat{a}]. \tag{6.16}$$

The degree of squeezing measured from the noise voltages from the balanced homodyne detector can be directly related to the spectrum of squeezing if there is no loss except through a single-output port [146]. Wu *et al.* [17] operated with a pump power well below the 30 mW threshold for optical parametric oscillation to prevent subharmonic light being reconverted to pump wavelengths. They were able to study the variation of the squeezing spectrum with pump power, and to measure $\langle(\Delta X)^2\rangle$ and $\langle(\Delta Y)^2\rangle$, and they verified that the squeezing was of a minimum-uncertainty type. This experiment truly represented the manipulation of the basic commutation relations of quantized light fields.

7. Applications

The experimental successes in generating light with significant amounts of squeezing bring closer the use of such light in various applications, whose potential importance has provided much of the stimulus for work in this area.

The earliest application to be considered was the reduction of quantum noise in optical communications [12, 110]. Thus if the operator $\hat{E}(\chi)$ in equation (5.17) represents the field of an information-carrying signal, the signal-to-noise ratio for balanced homodyne detection obtained from equations (5.34) and (5.35) is

$$\frac{S^2}{N}\equiv\frac{\langle m_{12}\rangle^2}{\langle(\Delta m_{12})^2\rangle}=\frac{4\eta\langle\hat{E}(\chi)\rangle^2}{1+\eta[4\langle(\Delta E(\chi))^2\rangle-1]}. \tag{7.1}$$

The field variance for squeezed light is given by equation (5.25) and the phase angle χ by equation (5.18), so that equation (7.1) becomes

$$\frac{S^2}{N}=\frac{4\eta|\alpha|^2\cos^2(\frac{1}{2}\theta-\phi)}{1-\eta+\eta\exp(-2s)}\quad\text{for}\quad\phi_L=\tfrac{1}{2}\theta+\tfrac{1}{2}\pi. \tag{7.2}$$

The denominator is equal to unity for coherent signal light ($s=0$), but it can in principle be made arbitrarily small for highly squeezed signal light ($s\to\infty$) with highly efficient photodetection ($\eta\to1$). Thus greatly enhanced signal-to-noise ratios are possible, with consequent advantages for optical communication systems. More

complete discussions of this application are given in [110, 112, 113]. It should be noted however that the squeezing of an optical signal is easily lost through the attenuation that occurs in transmission along a fibre and in attempts to compensate the loss by optical amplification [120], although it may be possible to overcome these problems to some extent by the use of further squeezed light sources to modify the transmission and amplification characteristics [63, 147]. Yamamoto and others [148–151] have examined the ways in which feedback in semiconductor lasers can lead to squeezing in active systems; such light sources could be of great value in applications to low-noise optical communications.

Another early proposal for the application of squeezed light was to facilitate the detection of gravitational waves by optical interferometry [14]. Such waves distort the interferometer, causing changes in optical path lengths, with resulting shifts in interference fringes that in principle enable the wave to be detected. The distortions and shifts expected in practice are extremely small, and they approach fundamental quantum limits on the minimum length resolution that can be achieved. It is found that the achievement of this optimum resolution requires the coherent light source of the interferometer to have an extremely high power. In considering the Michelson interferometer, Caves [14] showed that the power needed to achieve optimum resolution could be significantly reduced by the use of an auxiliary source of squeezed vacuum light shining into the interferometer via its telescope or detector arm. The quantum limit remains the same, but it can more readily be attained by this technique, which also applies to length measurements by other varieties of interferometer, for example the Fabry–Perot [152]. The practical implementation of squeezed light in gravitational-wave detection is discussed in detail in [153].

Several spectroscopic applications of squeezed light have been proposed. Thus Gardiner [154] has calculated the effect on atomic decay rates of replacing the normal vacuum environment by a squeezed-vacuum-state light beam, and Carmichael *et al.* [155] have determined the resonance fluorescence spectrum of a driven atom under similar conditions. The squeezed light can produce arbitrarily long relaxation times and spectral lines narrowed far below their natural widths. The Lamb shifts of spectral lines can also be changed from their normal values by irradiation of atoms with squeezed vacuum light [156]. Finally, it has been shown [157] that an order of magnitude improvement in sensitivity could in principle be achieved in frequency-modulation laser spectroscopy by the use of currently available detectors in conjunction with squeezing of the frequency modulation sidebands.

It is not clear at the time of writing which of these, or other, applications will show real practical benefits from the use of squeezed light, but the field of application is rich in promise. The range of interest in squeezing, extending from potentially useful applications to fundamental quantum-mechanical principles, seems certain to maintain a considerable research momentum for the foreseeable future.

Acknowledgments

We would like to thank F. A. M. de Oliveira for assistance with the figures, and Dr S. M. Barnett and Dr T. J. Shepherd for useful discussions. This work was supported in part by the U.K. Science and Engineering Research Council.

References

[1] WALLS, D. F., 1983, *Nature, Lond.*, **306,** 141.
[2] WALLS, D. F., and MILBURN, G. J., 1983, *Quantum Optics, Experimental Gravity and Measurement Theory*, edited by P. Meystre and M. O. Scully (New York: Plenum Press), p. 209.
[3] LEUCHS, G., 1985, *Non-Equilibrium Quantum Statistical Physics*, edited by G. Moore and M. O. Scully (New York: Plenum Press), p. 329.
[4] WALLS, D. F., and REID, M. D., 1986, *Frontiers in Quantum Optics*, edited by E. R. Pike and S. Sarkar (Bristol: Adam Hilger), p. 72.
[5] LOUDON, R., 1980, *Rep. Prog. Phys.*, **43,** 913.
[6] TAKAHASI, H., 1965, *Adv. Commun. Syst.*, **1,** 227.
[7] ROBINSON, D. R., 1965, *Commun. math. Phys.*, **1,** 159.
[8] STOLER, D., 1970, *Phys. Rev.* D, **1,** 3217.
[9] STOLER, D., 1971, *Phys. Rev.* D, **4,** 1925.
[10] LU, E. Y. C., 1971, *Lett. Nuovo Cim.*, **2,** 1241.
[11] LU, E. Y. C., 1972, *Lett. Nuovo Cim.*, **3,** 585.
[12] YUEN, H. P., 1976, *Phys. Rev.* A, **13,** 2226.
[13] HOLLENHORST, J. N., 1979, *Phys. Rev.* D, **19,** 1669.
[14] CAVES, C. M., 1981, *Phys. Rev.* D, **23,** 1693.
[15] SLUSHER, R. E., HOLLBERG, L. W., YURKE, B., MERTZ, J. C., and VALLEY, J. F., 1985, *Phys. Rev. Lett.*, **55,** 2409.
[16] SHELBY, R. M., LEVENSON, M. D., PERLMUTTER, S. H., DEVOE, R. G., and WALLS, D. F., 1986, *Phys. Rev. Lett.*, **57,** 691.
[17] WU, L.-A., KIMBLE, H. J., HALL, J. L., and WU, H., 1986, *Phys. Rev. Lett.*, **57,** 2520.
[18] SARGENT, M., SCULLY, M. O., and LAMB, W. E. JR., 1974, *Laser Physics* (Reading: Addison-Wesley).
[19] LOUDON, R., 1983, *The Quantum Theory of Light* (Oxford: Clarendon Press).
[20] GLAUBER, R. J., 1963, *Phys. Rev.*, **131,** 2766.
[21] KNIGHT, P. L., and ALLEN, L., 1983, *Concepts of Quantum Optics* (Oxford: Pergamon Press).
[22] MANDEL, L., 1979, *Optics Lett.*, **4,** 205.
[23] SUDARSHAN, E. C. G., 1963, *Phys. Rev. Lett.*, **10,** 277.
[24] MANDEL, L., 1986, *Physica scripta* T, **12,** 34.
[25] DALTON, B. J., 1986, *Physica scripta* T, **12,** 43.
[26] WIGNER, E. P., 1932, *Phys. Rev.*, **40,** 749.
[27] DRUMMOND, P. D., and GARDINER, C. W., 1980, *J. Phys.* A, **13,** 2353.
[28] MILBURN, G. J., and WALLS, D. F., 1983, *Am. J. Phys.*, **51,** 1134.
[29] HILLERY, M., and SCULLY, M. O., 1983, *Quantum Optics, Experimental Gravity and Measurement Theory*, edited by P. Meystre and M. O. Scully (New York: Plenum Press), p. 661.
[30] NIETO, M. M., 1985, *Non-equilibrium Quantum Statistical Physics*, edited by G. Moore and M. O. Scully (New York: Plenum Press), p. 287.
[31] STENHOLM, S., 1986, *Opt. Commun.*, **58,** 177.
[32] STENHOLM, S., 1986, *Physica scripta* T, **12,** 56.
[33] PEŘINOVÁ, V., KŘEPELKA, J., and PEŘINA, J., 1980, *Optica Acta*, **33,** 1263.
[34] FUJIWARA, T., and WERGELAND, H., 1984, *Essays in Theoretical Physics*, edited by W. E. Parry (Oxford: Pergamon Press), p. 313.
[35] SANDERS, B. C., BARNETT, S. M., and KNIGHT, P. L., 1986, *Opt. Commun.*, **58,** 290.
[36] MILBURN, G. J., 1984, *J. Phys.* A, **17,** 737.
[37] CAVES, C. M., and SCHUMAKER, B. L., 1985, *Phys. Rev.* D, **31,** 3068.
[38] COLLETT, M. J., and WALLS, D. F., 1985, *Phys. Rev.* A, **32,** 2887.
[39] COLLETT, M. J., and GARDINER, C. W., 1984, *Phys. Rev.* A, **30,** 1386.
[40] COLLETT, M. J., and LOUDON, R., 1987, *J. opt. Soc. Am.* B (to be published).
[41] COLLETT, M. J., LOUDON, R., and GARDINER, C. W., 1987, *J. mod. Opt.*, **34,** 881.
[42] MOLLOW, B. R., 1969, *Phys. Rev.*, **188,** 1969.
[43] SCHUDA, F., STROUD, C. R. JR., and HERCHER, M., 1974, *J. Phys.* B, **7,** L198.
[44] CARMICHAEL, H. J., and WALLS, D. F., 1976, *J. Phys.* B, **9,** L43.
[45] CARMICHAEL, H. J., and WALLS, D. F., 1976, *J. Phys.* B, **9,** 1199.

[46] COHEN-TANNOUDJI, D., 1977, *Frontiers in Laser Spectroscopy*, Vol. 1, edited by R. Balian, S. Haroche and S. Liberman (Amsterdam: North-Holland), p. 3.
[47] KIMBLE, H. J., and MANDEL, L., 1976, *Phys. Rev.* A, **13,** 2123.
[48] KIMBLE, H. J., DAGENAIS, M., and MANDEL, L., 1977, *Phys. Rev. Lett.*, **39,** 691.
[49] SHORT, R., and MANDEL, L., 1983, *Phys. Rev. Lett.*, **51,** 384.
[50] WALLS, D. F., and ZOLLER, P., 1981, *Phys. Rev. Lett.*, **47,** 709.
[51] ALLEN, L., and EBERLY, J. H., 1975, *Optical Resonance and Two-Level Atoms* (New York: John Wiley & Sons).
[52] TORREY, H. C., 1949, *Phys. Rev.*, **76,** 1059.
[53] BARNETT, S. M., 1987, *Opt. Commun.*, **61,** 432.
[54] WODKIEWICZ, K., KNIGHT, P. L., BUCKLE, S. M., and BARNETT, S. M., 1987, *Phys. Rev.* A, **35,** 2567.
[55] MANDEL, L., 1982, *Phys. Rev. Lett.*, **49,** 136.
[56] RADCLIFFE, J. M., 1971, *J. Phys.* A, **7,** 313.
[57] ARECCHI, F. T., COURTENS, E., GILMORE, R., and THOMAS, H., 1972, *Phys. Rev.* A, **6,** 2211.
[58] WODKIEWICZ, K., 1984, *Physics Lett.*, **51,** 198.
[59] WODKIEWICZ, K., and EBERLY, J. H., 1985, *J. opt. Soc. Am.* B, **2,** 458.
[60] HEIDMANN, A., and REYNAUD, S., 1985, *J. Phys., Paris*, **46,** 1937.
[61] VACCARO, J. A., and PEGG, D. T., 1986, *Optica Acta*, **33,** 1141.
[62] LOUDON, R., and SHEPHERD, T. J., 1984, *Optica Acta*, **31,** 1243.
[63] GILSON, C., BARNETT, S. M., and STENHOLM, S., 1987, *J. mod. Opt.*, **34,** 949.
[64] REID, M. D., WALLS, D. F., and DALTON, B. J., 1985, *Phys. Rev. Lett.*, **55,** 1288.
[65] SAVAGE, C. M., and WALLS, D. F., 1986, *Phys. Rev.* A, **33,** 3282.
[66] DALTON, B. J., and KNIGHT, P. L., 1982, *J. Phys.* B, **15,** 399.
[67] ALZETTA, G., GOZZINI, A., MOI, L., and ORRIOLS, G., 1976, *Nuovo Cim.* B, **36,** 5.
[68] ARIMONDO, E., and ORRIOLS, G., 1976, *Lett. Nuovo Cim.*, **17,** 333.
[69] ORRIOLS, G., 1979, *Nuovo Cim.* B, **53,** 1.
[70] ALZETTA, G., MOI, L., and ORRIOLS, G., 1979, *Nuovo Cim.* B, **52,** 209.
[71] GRAY, H. R., WHITLEY, R. M., and STROUD, C. R. JR., 1978, *Optics Lett.*, **3,** 218.
[72] RADMORE, P. M., and KNIGHT, P. L., 1982, *J. Phys.* B, **15,** 561.
[73] WALLS, D. F., and REID, M. D., 1986, *Frontiers in Quantum Optics*, edited by E. R. Pike and S. Sarkar (Bristol: Adam Hilger), p. 100.
[74] LANE, A. S., REID, M. D., SAVAGE, C. M., and WALLS, D. F., 1986, *J. opt. Soc. Am.*, **3,** P84.
[75] DE OLIVEIRA, F. A. M., DALTON, B. J., and KNIGHT, P. L., 1987, *J. opt. Soc. Am.* B (to be published).
[76] CORNEY, A., 1977, *Atomic and Laser Spectroscopy* (Oxford University Press), Chap. 15.
[77] ANANTHA LAKSHMI, P., and AGARWAL, G. S., 1985, *Phys. Rev.* A, **32,** 1643.
[78] CARMICHAEL, H. J., 1985, *Phys. Rev. Lett.*, **55,** 2790.
[79] BUTLER, M., and DRUMMOND, P. D., 1986, *Optica Acta*, **33,** 1.
[80] KIMBLE, H. J., 1986, *Frontiers in Quantum Optics*, edited by E. R. Pike and S. Sarkar (Bristol: Adam Hilger), p. 521.
[81] HAROCHE, S., and RAIMOND, J. M., 1985, *Advances in Atomic and Molecular Physics*, Vol. 20, edited by D. R. Bates and B. Bederson (London: Academic Press), p. 350.
[82] GALLAS, J. A. C., LEUCHS, G., WALTHER, H., and FIGGER, H., 1985, *Advances in Atomic and Molecular Physics*, Vol. 20, edited by D. R. Bates and B. Bederson (London: Academic Press), p. 414.
[83] HAROCHE, S., 1984, *New Trends in Atomic Physics*, edited by G. Grynberg and R. Stora (Amsterdam: North-Holland), p. 193.
[84] MESCHEDE, D., WALTHER, H., and MULLER, G., 1985, *Phys. Rev. Lett.*, **54,** 551.
[85] FILIPOWICZ, P., MEYSTRE, P., REMPE, G., and WALTHER, H., 1985, *Optica Acta*, **32,** 1105.
[86] BARNETT, S. M., FILIPOWICZ, P., JAVANAINEN, J., KNIGHT, P. L., and MEYSTRE, P., 1986, *Frontiers in Quantum Optics*, edited by E. R. Pike and S. Sarkar (Bristol: Adam Hilger), p. 485.
[87] REMPE, G., WALTHER, H., and KLEIN, N., 1987, *Phys. Rev. Lett.*, **58,** 353.
[88] KNIGHT, P. L., 1986, *Physica scripta* T, **12,** 51.
[89] KRAUSE, J., SCULLY, M. O., and WALTHER, H., 1986, *Phys. Rev.* A, **34,** 2032.

[90] HEIDMANN, A., RAIMOND, J. M., and REYNAUD, S., 1985, *Phys. Rev. Lett.*, **54,** 326.
[91] HEIDMANN, A., RAIMOND, J. M., REYNAUD, S., and ZAGURY, N., 1985, *Opt. Commun.*, **54,** 54.
[92] HEIDMANN, A., RAIMOND, J. M., REYNAUD, S., and ZAGURY, N., 1985, *Opt. Commun.*, **54,** 189.
[93] HEIDEMANN, A., and REYNAUD, S., 1987, *J. mod. Opt.*, **34,** 923.
[94] ANANTHA LAKSHMI, P., and AGARWAL, G. S., 1980, *Opt. Commun.*, **51,** 425.
[95] JAYNES, E. T., and CUMMINGS, F. W., 1963, *Proc. IEEE*, **51,** 89.
[96] MEYSTRE, P., GENEUX, E., FAIST, A., and QUATTROPANI, A., 1975, *Nuovo Cimento*, **25B,** 251.
[97] VON FOERSTER, T., 1975, *J. Phys.* A, **8,** 95.
[98] CUMMINGS, F. W., 1965, *Phys. Rev.*, **140,** A1051.
[99] EBERLY, J. H., SANCHEZ-MONDRAGON, J. J., and NAROZHNY, N. B., 1980, *Phys. Rev. Lett.*, **44,** 1323.
[100] NAROZHNY, N. B., SANCHEZ-MONDRAGON, J. J., and EBERLY, J. H., 1981, *Phys. Rev.* A, **23,** 236.
[101] YOO, H. I., SANCHEZ-MONDRAGON, J. J., and EBERLY, J. H., 1981, *J. Phys.* A, **14,** 1383.
[102] KNIGHT, P. L., and RADMORE, P. M., 1982, *Phys. Rev.* A, **26,** 676.
[103] KNIGHT, P. L., and RADMORE, P. M., 1982, *Phys. Lett.*, **90A,** 342.
[104] BARNETT, S. M., and KNIGHT, P. L., 1986, *Phys. Rev.* A, **33,** 2444.
[105] PURI, R. R., and AGARWAL, G. S., 1986, *Phys. Rev.* A, **33,** 3610.
[106] MEYSTRE, P., and ZUBAIRY, M. S., 1982, *Phys. Lett.*, **89A,** 390.
[107] MILBURN, G., 1984, *Optica Acta*, **31,** 671.
[108] FILIPOWICZ, P., JAVANAINEN, J., and MEYSTRE, P., 1986, *Opt. Commun.*, **58,** 327.
[109] FILIPOWICZ, P., JAVANAINEN, J., and MEYSTRE, P., 1986, *Phys. Rev.* A, **34,** 3077.
[110] YUEN, H. P., and SHAPIRO, J. H., 1980, *IEEE Trans. Inf. Theory*, **26,** 78.
[111] WALLS, D. F., MILBURN, G. J., and CARMICHAEL, H. J., 1982, *Optica Acta*, **29,** 1179; 1982, *Ibid.*, **29,** 1453 (erratum).
[112] YUEN, H. P., and SHAPIRO, J. H., 1978, *IEEE Trans. Inf. Theory*, **24,** 657.
[113] SHAPIRO, J. H., YUEN, H. P., and MACHADO, MATA, J. A., 1979, *IEEE Trans. Inf. Theory*, **25,** 179.
[114] LOUDON, R., 1986, *Quantum Optics IV*, edited by J. D. Harvey and D. F. Walls (Berlin: Springer), p. 70.
[115] YUEN, H. P., and CHAN, V. W. S., 1983, *Optics Lett.*, **8,** 177.
[116] SCHUMAKER, B. L., 1984, *Optics Lett.*, **9,** 189.
[117] WALKER, N. G., and CARROLL, J. E., 1986, *Opt. quantum Electron.*, **18,** 355.
[118] WALKER, N. G., 1987, *J. mod. Opt.*, **34,** 15.
[119] ARTHURS, E., and KELLY, J. L., 1965, *Bell Syst. tech. J.*, **44,** 725.
[120] LOUDON, R., 1986, *Frontiers in Quantum Optics*, edited by E. R. Pike and S. Sarkar (Bristol: Adam Hilger), p. 42.
[121] BANDILLA, A., 1977, *Opt. Commun.*, **23,** 299.
[122] YUEN, H. P., and SHAPIRO, J. H., 1979, *Optics Lett.*, **4,** 334.
[123] REYNAUD, S., and HEIDMANN, A., 1984, *Opt. Commun.*, **50,** 271.
[124] REID, M. D., and WALLS, D. F., 1984, *Opt. Commun.*, **50,** 406.
[125] REID, M. D., and WALLS, D. F., 1985, *Phys. Rev.* A, **31,** 1622.
[126] KOZIEROWSKI, M., and TANAŚ, R., 1977, *Opt. Commun.*, **21,** 229.
[127] MANDEL, L., 1982, *Opt. Commun.*, **42,** 437.
[128] LUGIATO, L., STRINI, G., and DE MARTINI, F., 1983, *Optics Lett.*, **8,** 256.
[129] DRUMMOND, P. D., MCNEIL, K. J., and WALLS, D. F., 1980, *Optica Acta*, **27,** 321.
[130] MILBURN, G. J., and WALLS, D. F., 1981, *Opt. Commun.*, **39,** 401.
[131] MILBURN, G. J., and WALLS, D. F., 1983, *Phys. Rev.* A, **27,** 392.
[132] LUGIATO, L. A., and STRINI, G., 1982, *Opt. Commun.*, **41,** 67.
[133] LANE, A., TOMBESI, P., CARMICHAEL, H. J., and WALLS, D. F., 1983, *Opt. Commun.*, **48,** 155.
[134] WODKIEWICZ, K., and ZUBAIRY, M. S., 1983, *Phys. Rev.* A, **27,** 2003.
[135] DRUMMOND, P. D., MCNEIL, K. J., and WALLS, D. F., 1980, *Optica Acta*, **28,** 211.
[136] LUGIATO, L. A., and STRINI, G., 1982, *Opt. Commun.*, **41,** 374.
[137] LUGIATO, L. A., and STRINI, G., 1982, *Opt. Commun.*, **41,** 447.

[138] REID, M. D., and WALLS, D. F., 1983, *Phys. Rev.* A, **28,** 332.
[139] LOUDON, R., 1984, *Opt. Commun.*, **49,** 67.
[140] YURKE, B., 1984, *Phys. Rev.* A, **29,** 408.
[141] GARDINER, C. W., and SAVAGE, C. M., 1984, *Opt. Commun.*, **50,** 173.
[142] YURKE, B., 1985, *Phys. Rev.* A, **32,** 300.
[143] YURKE, B., 1985, *Phys. Rev.* A, **32,** 311.
[144] LEVENSON, M. D., SHELBY, R. M., REID, M. D., WALLS, D. F., and ASPECT, A., 1985, *Phys. Rev.* A, **32,** 1550.
[145] SHELBY, R. M., LEVENSON, M. D., WALLS, D. F., ASPECT, A., and MILBURN, G. J., 1986, *Phys. Rev.* A, **33,** 4008.
[146] SHAPIRO, J. H., 1985, *IEEE Jl quant. Electron.*, **21,** 237.
[147] VACCARO, J. A., and PEGG, D. T., 1987, *J. mod. Opt.*, **34,** 855.
[148] YAMAMOTO, Y., IMOTO, N., and MACHIDA, S., 1986, *Phys. Rev.* A, **33,** 3243.
[149] HAUS, H. A., and YAMAMOTO, Y., 1986, *Phys. Rev.* A, **34,** 270.
[150] CARROLL, J. E., 1986, *Optica Acta*, **33,** 909.
[151] MACHIDA, S., YAMAMOTO, Y., and ITAYA, Y., 1987, *Phys. Rev. Lett.*, **58,** 1000.
[152] LEY, M., and LOUDON, R., 1987, *J. mod. Opt.*, **34,** 227.
[153] GEA-BANACLOCHE, J., and LEUCHS, G., 1987, *J. mod. Opt.*, **34,** 793.
[154] GARDINER, C. W., 1986, *Phys. Rev. Lett.*, **56,** 1917.
[155] CARMICHAEL, H. J., LANE, A. S., and WALLS, D. F., 1987, *J. mod. Opt.*, **34,** 821.
[156] MILBURN, G. J., 1986, *Phys. Rev.* A, **34,** 4882.
[157] YURKE, B., and WHITTAKER, E. A., 1987, *Optics Lett.*, **12,** 236.